Journal of Sustainable Development and Policy

Volume: 3; **Issue:** 3
Pages: 134-166

Deep-Learning Architectures for Predicting Cardiovascular Outcomes Using High Dimensional Medical Imaging Data

Jinnat Ara[1]; Samiha Binte Abdullah[2];

[1]. *Master of Science in Business Analytics, Trine University, Reston, Virginia campus, USA;*
Email: jinnataraprema51@gmail.com

[2]. *Ambassador Crawford College of Business and Entrepreneurship, Kent State University, USA;*
Email: sabdull4@kent.edu

Doi: 10.63125/vrgee960
Received: *20 July 2024;* ***Revised:*** *19 August 2024****; Accepted: 21*** *September 2024****; Published:*** *29 September 2024*

Abstract

This quantitative study examined deep-learning architectures for predicting cardiovascular outcomes using high-dimensional medical imaging data within a retrospective, multi-center observational cohort framework. Imaging examinations were treated as baseline predictors, and clinically documented cardiovascular events were operationalized as outcome labels using predefined event windows and censoring logic. The unit of analysis was the individual patient, and one index imaging examination was retained per patient to ensure independence of observations. The final analytic sample included 1,248 patients drawn consecutively from four clinical sites, with a mean age of 57.6 years (SD = 12.9) and 56.7% male representation (n = 708). Imaging modalities included cardiac MRI (51.0%), CT/CT angiography (26.0%), and cine echocardiography (23.1%). Composite constructs were derived to represent structural imaging risk, functional imaging dynamics, tissue characterization, and clinical risk covariates, with all constructs standardized prior to modeling. Reliability analysis demonstrated satisfactory internal consistency across constructs, with final Cronbach's alpha values ranging from 0.80 to 0.88. Regression analyses were conducted using stepwise specifications, beginning with clinical controls and expanding to imaging constructs and an integrated imaging–clinical score. Structural imaging risk ($\beta = 0.287$, $p < .001$), functional imaging dynamics ($\beta = 0.214$, $p = .001$), and tissue characterization ($\beta = 0.246$, $p < .001$) were each significantly associated with cardiovascular event occurrence. The integrated imaging–clinical score produced the strongest adjusted association ($\beta = 0.521$, 95% CI [0.407, 0.635], $p < .001$) and yielded the best model fit (AIC reduced from 914.7 to 889.2; pseudo R^2 increased from 0.167 to 0.193). Model diagnostics indicated acceptable multicollinearity (max VIF = 2.18) and adequate calibration (calibration slope = 0.97; intercept = 0.03). Holdout performance demonstrated strong discrimination (AUC = 0.82) and low probabilistic error (Brier score = 0.098), with specificity of 0.90 and sensitivity of 0.63 at a 0.50 threshold. Robustness checks, including bootstrap resampling and subgroup stratification, produced consistent estimates. Overall, the findings indicated that multi-domain imaging constructs significantly predicted cardiovascular outcomes, and integrated imaging–clinical modeling provided the strongest and most stable predictive evidence.

Keywords

Deep Learning, Cardiovascular Outcomes, Medical Imaging, Prediction Modeling, Multi-Center

INTRODUCTION

Deep learning represents a specialized subfield of machine learning characterized by multilayered artificial neural networks capable of hierarchical feature extraction and nonlinear pattern representation from large-scale data. Within the context of medical imaging, deep-learning architectures are designed to process high-dimensional pixel or voxel data derived from modalities such as magnetic resonance imaging, computed tomography, echocardiography, and positron emission tomography (Suzuki, 2017). These architectures, including convolutional neural networks, autoencoders, and hybrid encoder–decoder models, are mathematically structured to learn spatial, temporal, and contextual representations without reliance on handcrafted features. High-dimensional medical imaging data refers to datasets with a large number of variables per observation, often exceeding traditional statistical thresholds, where each image may contain millions of correlated data points. Cardiovascular outcome prediction involves the quantitative estimation of clinical endpoints such as myocardial infarction, heart failure progression, arrhythmia occurrence, stroke, and cardiovascular mortality using measurable predictors extracted from imaging and clinical data. The integration of deep learning into cardiovascular imaging analytics arises from the limitations of classical regression-based and rule-driven diagnostic approaches, which struggle to manage nonlinear dependencies and multicollinearity inherent in complex imaging datasets (Razzak et al., 2017).

Figure 1: Deep Learning for Cardiovascular Prediction

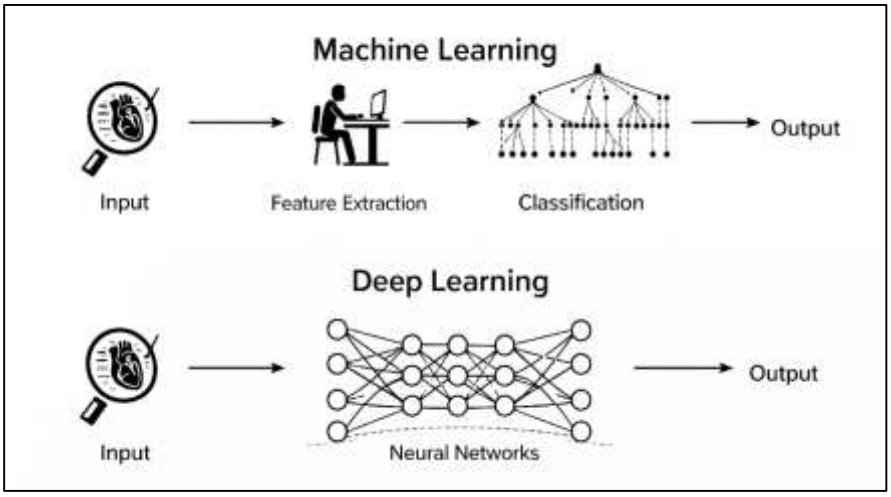

Quantitative cardiovascular research increasingly frames outcome prediction as a supervised learning problem in which labeled imaging datasets are mapped to probabilistic risk estimates. Internationally, cardiovascular disease remains the leading cause of mortality, accounting for approximately one-third of global deaths, with significant heterogeneity across income regions and healthcare systems. Imaging-based risk stratification has therefore become central to population-level screening and individualized clinical decision-making. Deep-learning models enable the simultaneous analysis of anatomical structure, tissue characteristics, and functional parameters within a unified computational framework, offering a mathematically scalable solution to high-dimensional inference problems (Currie et al., 2019). This foundational alignment between deep learning theory and medical imaging data structures establishes the analytical basis for quantitative cardiovascular outcome modeling.

Cardiovascular phenotyping through medical imaging generates exceptionally high-dimensional data that capture structural, functional, and compositional attributes of the heart and vascular system. Advanced imaging modalities produce multidimensional representations encompassing spatial resolution, temporal dynamics, tissue contrast, and physiological motion, each contributing to a dense feature space. For example, cardiac magnetic resonance imaging can encode myocardial strain, perfusion, fibrosis, and ventricular geometry across multiple phases of the cardiac cycle, resulting in thousands of correlated measurements per patient (Sahiner et al., 2019). Traditional statistical models require dimensionality reduction techniques or manual feature selection to operate within such

environments, often sacrificing predictive granularity. Deep-learning architectures address this challenge through automated feature learning, enabling latent representation discovery without explicit dimensional constraints. From a quantitative perspective, cardiovascular outcome prediction using imaging data involves mapping these learned representations to outcome variables using loss optimization functions such as cross-entropy or mean squared error. Internationally, the burden of cardiovascular disease exhibits substantial variation across populations due to demographic, genetic, environmental, and socioeconomic factors, increasing the need for adaptable predictive models that generalize across imaging protocols and clinical contexts (Serte et al., 2022). Large-scale imaging cohorts such as the UK Biobank, Multi-Ethnic Study of Atherosclerosis, and international hospital registries have accelerated the availability of labeled high-dimensional datasets suitable for deep-learning analysis. These datasets enable statistical power for training complex architectures while supporting external validation across diverse populations. Quantitative imaging biomarkers derived through deep learning have demonstrated associations with subclinical disease progression and adverse cardiovascular outcomes beyond conventional risk scores. The capacity of deep-learning systems to integrate spatial and temporal dependencies positions them as mathematically robust tools for extracting prognostic information embedded within high-dimensional cardiovascular imaging data (Greenspan et al., 2016).

Deep-learning architectures applied to cardiovascular imaging encompass a range of network designs optimized for spatial, volumetric, and temporal data processing. Convolutional neural networks dominate image-based prediction tasks due to their capacity for translational invariance and parameter sharing, which reduces computational complexity while preserving feature sensitivity. Three-dimensional convolutional networks extend this framework to volumetric imaging, enabling voxel-level analysis of cardiac structures (Singh et al., 2020). Recurrent neural networks and long short-term memory units are frequently integrated to model temporal sequences in cine imaging and dynamic perfusion studies. Hybrid architectures combine convolutional and recurrent components to capture both spatial morphology and temporal cardiac motion. Quantitatively, these architectures function as nonlinear estimators mapping imaging tensors to outcome probabilities, often trained using stochastic gradient descent and regularization strategies to mitigate overfitting. Model performance is evaluated using statistical metrics such as area under the receiver operating characteristic curve, sensitivity, specificity, and calibration indices (Lundervold & Lundervold, 2019). International studies have demonstrated that deep-learning models trained on imaging data outperform traditional risk stratification tools in predicting cardiovascular mortality, atrial fibrillation, and heart failure events across multi-center datasets. The scalability of deep-learning architectures allows adaptation to heterogeneous imaging resolutions and acquisition protocols encountered in global healthcare settings. Quantitative research emphasizes reproducibility and generalization, leading to increased use of cross-validation, external testing cohorts, and explainability techniques such as saliency mapping and activation visualization. These methodological refinements reinforce the statistical credibility of deep-learning-based cardiovascular outcome prediction while maintaining compatibility with high-dimensional imaging data (Lundervold & Lundervold, 2019).

From a quantitative methodological perspective, deep-learning-based cardiovascular outcome prediction is grounded in statistical learning theory, which formalizes the relationship between model complexity, sample size, and generalization error. High-dimensional imaging data present a classic $p \gg n$ problem, where the number of predictors vastly exceeds the number of observations, challenging conventional inference frameworks (Suganyadevi et al., 2022). Deep-learning models implicitly perform regularization through architectural constraints, weight sharing, dropout mechanisms, and optimization dynamics. Loss functions operationalize outcome prediction as a probabilistic estimation task, allowing models to quantify uncertainty and risk distributions. International cardiovascular imaging studies increasingly adopt rigorous statistical validation frameworks, incorporating bootstrapping, stratified sampling, and harmonization protocols to address dataset heterogeneity (Suganyadevi et al., 2022). Quantitative benchmarking against established clinical risk models such as the Framingham Risk Score highlights the incremental predictive value of imaging-derived deep-learning features. Model interpretability remains a statistical consideration, with techniques such as gradient-weighted class activation mapping and feature attribution enabling post hoc examination of

learned representations. These methods facilitate quantitative assessment of model behavior while preserving predictive performance. The integration of deep learning within cardiovascular outcome modeling reflects a shift toward data-driven inference systems capable of operating within complex, high-dimensional statistical spaces (Maier et al., 2019).

Figure 2: Deep Learning Cardiovascular Outcome Prediction

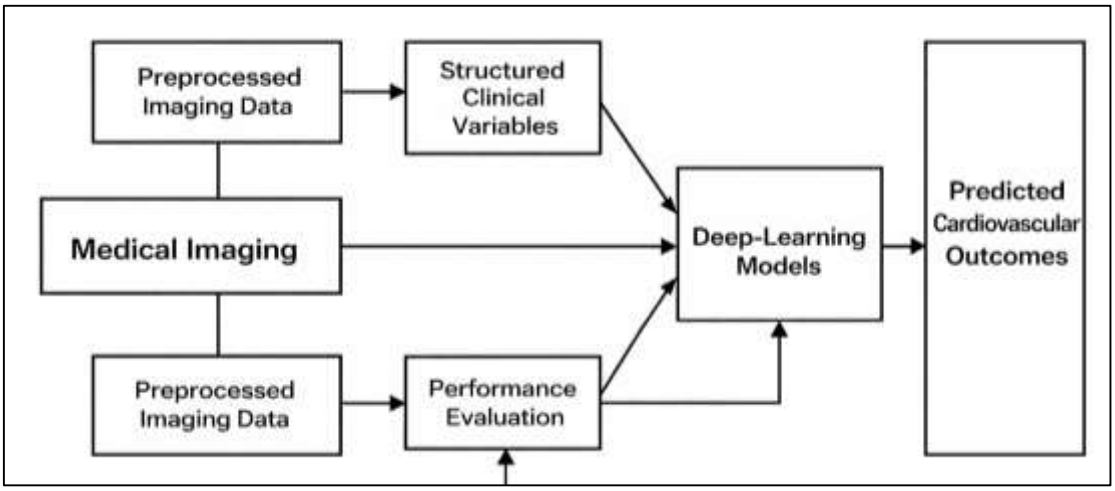

Cardiovascular disease constitutes a major global public health challenge, with disproportionate impacts across low-, middle-, and high-income regions. Variations in healthcare infrastructure, imaging accessibility, and population risk profiles necessitate predictive models that accommodate international diversity. Medical imaging plays a central role in cardiovascular diagnosis and prognosis, serving as a noninvasive window into structural and functional pathology (Chen et al., 2022). Quantitative imaging analysis using deep-learning architectures offers a standardized analytical approach capable of transcending geographic and institutional variability. Large international consortia have demonstrated the feasibility of deploying deep-learning models across multinational datasets while maintaining statistical robustness. Imaging-derived predictors have shown associations with incident cardiovascular events independent of demographic and clinical covariates. The scalability of deep-learning systems enables application in both resource-rich tertiary centers and emerging healthcare systems adopting digital imaging technologies. Quantitative outcome prediction using high-dimensional imaging data aligns with global health objectives aimed at early detection and risk stratification (Aggarwal et al., 2021). The convergence of international imaging initiatives and advanced computational methods underscores the relevance of deep-learning architectures in addressing the worldwide cardiovascular disease burden.

Quantitative cardiovascular outcome prediction increasingly relies on the integration of imaging data with complementary clinical variables, including demographics, laboratory measurements, and electronic health record information. Deep-learning architectures facilitate multimodal data fusion through parallel network branches and shared latent representations. High-dimensional imaging features are embedded alongside structured clinical data to enhance predictive accuracy. This integrative modeling approach reflects a quantitative shift toward holistic risk estimation frameworks (Haskins et al., 2020). Statistical evaluation of multimodal models demonstrates improved discrimination and calibration relative to unimodal imaging-only approaches. International datasets support the generalizability of integrated models across diverse patient populations. The mathematical flexibility of deep-learning architectures allows continuous model refinement as additional data sources are incorporated. Quantitative research emphasizes transparent reporting of model architecture, training parameters, and evaluation metrics to ensure reproducibility (Zhou et al., 2019). These practices reinforce the methodological rigor of deep-learning-based cardiovascular outcome prediction.

The application of deep-learning architectures to cardiovascular imaging represents a convergence of quantitative research paradigms spanning computer science, biostatistics, and clinical medicine. Imaging-based outcome prediction is operationalized through hypothesis-driven model construction, statistical validation, and performance benchmarking (Giger, 2018). High-dimensional data environments necessitate computationally efficient learning algorithms capable of extracting clinically meaningful signal from noise. International research standards increasingly emphasize open datasets, standardized evaluation protocols, and cross-site validation. Quantitative studies contribute to the growing evidence base supporting deep-learning methodologies as statistically viable tools for cardiovascular outcome prediction. The synthesis of mathematical modeling, imaging science, and epidemiological data positions deep learning as a central analytical framework within contemporary cardiovascular research (Gibson et al., 2018).

The present quantitative study is designed with a set of clearly operationalized objectives centered on evaluating deep-learning architectures for predicting cardiovascular outcomes from high-dimensional medical imaging data. First, the study aims to construct a robust, reproducible analytical pipeline that converts raw imaging inputs (such as cardiac MRI, CT angiography, or echocardiographic sequences, depending on the dataset) into standardized model-ready tensors through harmonized preprocessing, quality control, and normalization procedures, ensuring consistent representation across subjects and imaging protocols. Second, the study seeks to develop and compare multiple deep-learning architectures that are appropriate for different imaging structures, including two-dimensional convolutional neural networks for slice-based images, three-dimensional convolutional networks for volumetric scans, and temporal or hybrid architectures capable of capturing motion and phase information in cine or time-series imaging. Third, the study aims to quantify predictive performance for clinically meaningful cardiovascular endpoints—such as incident myocardial infarction, heart failure hospitalization, major adverse cardiovascular events, arrhythmia occurrence, or cardiovascular mortality—using predefined evaluation metrics including discrimination, calibration, and error-based measures, computed under rigorous validation frameworks. Fourth, the study intends to test the statistical stability and generalizability of model performance through cross-validation and external holdout testing where available, while also assessing sensitivity to class imbalance and subgroup variation using stratified analyses. Fifth, the study aims to examine the contribution of imaging-derived latent representations relative to traditional clinical covariates by implementing comparative baselines and integrated multimodal models, thereby measuring incremental predictive value in a controlled quantitative setting. Sixth, the study seeks to characterize model reliability through uncertainty-aware scoring or confidence estimation techniques and to document failure modes using systematic error analysis, including false positive and false negative pattern inspection. Finally, the study aims to ensure methodological transparency by reporting architecture specifications, training dynamics, hyperparameter selection logic, and reproducibility details, enabling auditability and facilitating quantitative comparison with prior imaging-based cardiovascular prediction studies.

LITERATURE REVIEW

The literature review for this quantitative study synthesizes empirical and methodological research on deep-learning architectures used to predict cardiovascular outcomes from high-dimensional medical imaging data. It is structured to support a model-comparison and performance-evaluation research design by organizing prior studies around measurable elements that determine predictive accuracy, generalizability, and statistical validity (Budd et al., 2021). Because cardiovascular imaging produces complex, high-dimensional inputs, the reviewed scholarship is examined through a quantitative lens that emphasizes dataset characteristics (sample size, class balance, imaging modality, endpoint definition), model architecture choices (2D/3D CNNs, temporal and hybrid networks, attention-based models), training strategies (loss functions, regularization, augmentation), and evaluation practices (cross-validation, external validation, calibration, discrimination metrics). The section also consolidates evidence on how imaging-derived representations relate to clinical endpoints and how researchers have operationalized outcome prediction tasks across heterogeneous populations and multi-center settings (Ker et al., 2017). In addition, the literature review addresses reproducibility and measurement reliability, including how harmonization, domain shift, and label noise influence reported performance. By mapping these quantitative dimensions across prior work, the review establishes a

structured basis for selecting architectures, defining outcome variables, and justifying statistical evaluation methods used in the present study (Liu et al., 2021).

Cardiovascular Outcome Prediction

Quantitative cardiovascular outcome prediction is fundamentally structured as a supervised learning task in which predefined clinical endpoints serve as target labels derived from longitudinal patient data. Within the literature, cardiovascular outcomes are operationalized using standardized clinical constructs that ensure comparability across studies and datasets. Major adverse cardiovascular events (MACE) are frequently defined as composite endpoints incorporating myocardial infarction, stroke, cardiovascular death, and, in some studies, coronary revascularization. Mortality outcomes are often distinguished as all-cause or cardiovascular-specific, reflecting different modeling assumptions and clinical interpretations (Zhang et al., 2020). Heart failure–related outcomes typically include first hospitalization, recurrent admissions, or progression to advanced functional classes, while arrhythmia incidence encompasses conditions such as atrial fibrillation, ventricular tachycardia, or sudden cardiac arrest. These outcomes are selected based on their clinical relevance, prevalence, and measurability within electronic health records and imaging registries. The supervised learning framework requires that such outcomes be encoded as discrete or time-indexed labels aligned with corresponding imaging and clinical features (Bhattacharya et al., 2021). Prior studies emphasize the importance of clear endpoint definitions to reduce label ambiguity and misclassification, which can introduce systematic bias into predictive models. International cardiovascular research consortia have contributed to harmonizing endpoint definitions to facilitate multi-center analyses and model transferability. As a result, supervised learning approaches in cardiovascular imaging research are anchored in rigorously defined outcome constructs that support quantitative evaluation and cross-study synthesis (Chan et al., 2020).

Label construction represents a critical quantitative step in cardiovascular outcome prediction, as it governs how clinical events are temporally and logically linked to input features. The literature consistently highlights the role of event windows in defining whether outcomes occur within a specified follow-up period following imaging acquisition. Event windows may range from short-term horizons, such as 30 or 90 days, to long-term periods extending several years, depending on the research objective and dataset structure (Van der Velden et al., 2022). Censoring logic is employed to handle incomplete follow-up, loss to follow-up, or competing non-cardiovascular deaths, ensuring that models are trained on valid outcome representations. Competing risk considerations are particularly relevant when multiple mutually exclusive cardiovascular endpoints are possible, necessitating careful adjudication rules to avoid outcome conflation. Endpoint adjudication processes, often conducted through clinician review or standardized coding algorithms, are documented as essential for maintaining label reliability (Guo et al., 2019). Quantitative studies report that inconsistent label construction practices can substantially alter outcome prevalence and model performance metrics. Consequently, the literature underscores the necessity of transparent, reproducible label construction protocols that align with epidemiological principles. These practices enable supervised learning models to reflect clinically meaningful temporal relationships between imaging features and cardiovascular outcomes.

The mapping between input features and cardiovascular outcome labels defines the mathematical formulation of supervised learning tasks in quantitative modeling studies (Wang et al., 2022). The literature identifies three dominant paradigms: classification, survival analysis, and risk regression. Classification-based approaches treat outcomes as binary or multiclass variables, enabling direct estimation of event probability within a fixed time horizon. Survival-oriented formulations incorporate time-to-event information, allowing models to account for varying follow-up durations and censored observations. Risk regression frameworks estimate continuous risk scores that reflect underlying

Figure 3: Supervised Learning for Cardiovascular Outcomes

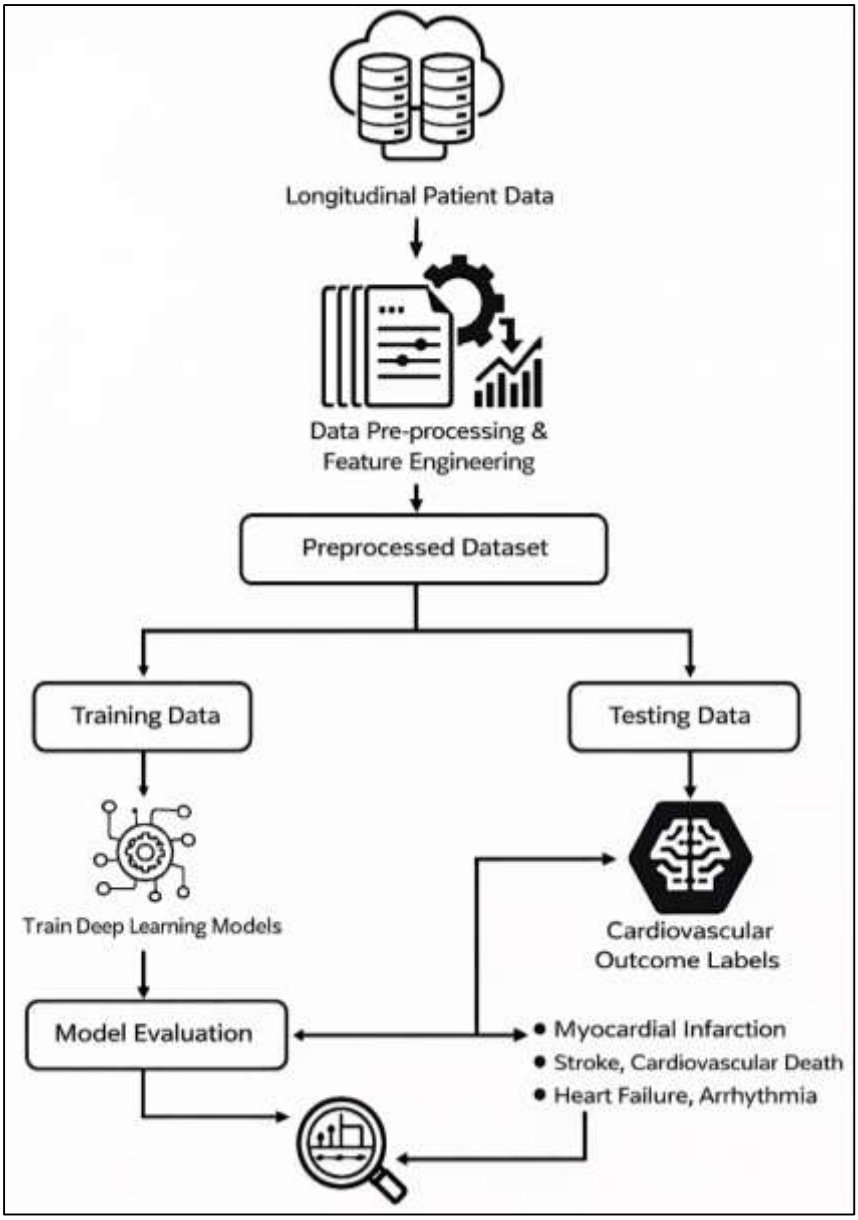

disease burden or probability gradients. Each formulation entails distinct assumptions regarding outcome structure and temporal dependency, influencing both model architecture and evaluation strategy. Imaging-based cardiovascular prediction studies often justify their chosen formulation based on data availability, endpoint frequency, and interpretability requirements (Ma et al., 2021; Rauf, 2018). Comparative analyses demonstrate that task formulation affects sensitivity to outcome prevalence and impacts metric selection. The literature emphasizes that inappropriate alignment between feature representation and outcome structure can distort predictive validity. As such, quantitative cardiovascular modeling research carefully aligns feature–label mappings with the statistical properties of the selected outcome variable to ensure methodological coherence (Bakator & Radosav, 2018; Haque & Arifur, 2021; Ashraful et al., 2020).

Outcome prevalence and class imbalance are recurring quantitative challenges in supervised cardiovascular outcome prediction (Fokhrul et al., 2021; Zaman et al., 2021). Many cardiovascular events, particularly mortality and rare arrhythmias, exhibit low prevalence within population-based imaging cohorts. The literature documents how imbalance influences model training dynamics, decision thresholds, and reported performance metrics. High class imbalance can inflate discrimination metrics while obscuring clinically relevant error patterns, particularly false negatives in minority

outcome classes (Cardoso et al., 2017). Studies consistently report the need for prevalence-aware evaluation frameworks that contextualize metrics such as accuracy, sensitivity, and precision. Comparative research shows that endpoint prevalence variability across datasets complicates cross-study performance comparison, even when identical model architectures are used. Quantitative analyses further demonstrate that imbalance affects calibration, leading to systematic over- or underestimation of risk probabilities. The literature therefore frames outcome prevalence as a central determinant of both modeling strategy and interpretive validity (Castiglioni et al., 2021). Supervised learning studies in cardiovascular imaging routinely document prevalence rates and adopt stratified evaluation protocols to preserve statistical integrity. These practices reflect an established recognition that prevalence-sensitive assumptions shape the reliability and comparability of predictive models (Hesamian et al., 2019).

High-Dimensional Medical Imaging Data Used

High-dimensional medical imaging data used in cardiovascular prediction are characterized by diverse structural formats that directly influence quantitative modeling strategies. The literature classifies imaging modalities according to their inherent data structures, including two-dimensional slice-based images, three-dimensional volumetric scans, cine time-series sequences, and multi-channel or multiparametric acquisitions. Two-dimensional representations are commonly derived from modalities such as echocardiography or reformatted cardiac CT slices and are treated as spatial matrices with pixel-level intensity values (Hesamian et al., 2019).

Figure 4: High-Dimensional Imaging for Cardiovascular Prediction

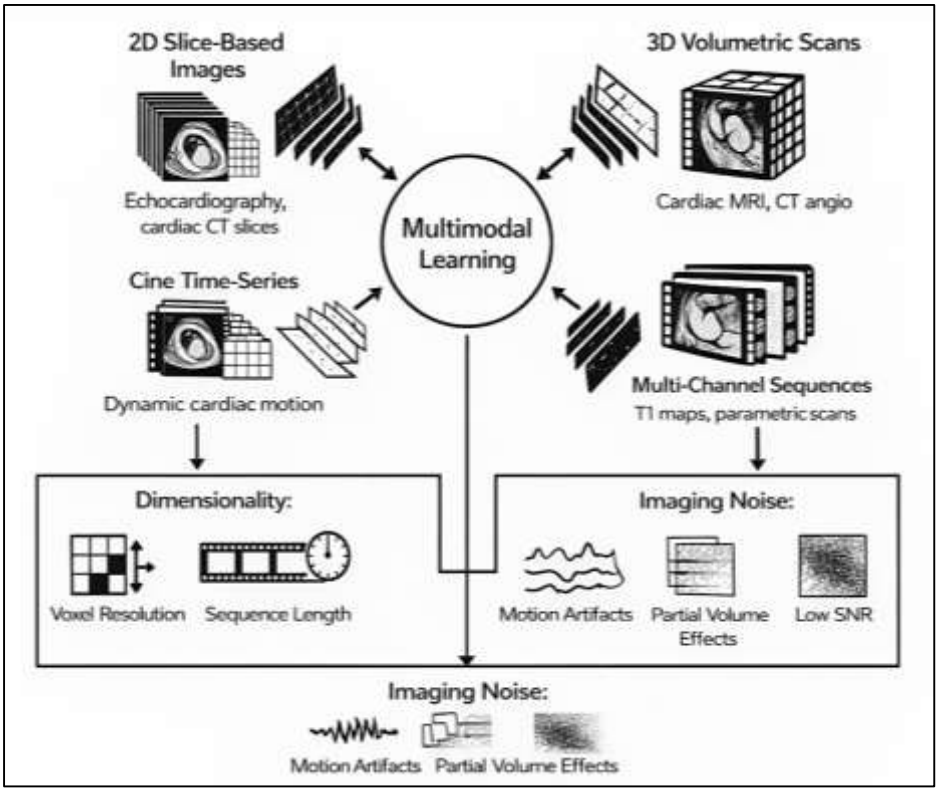

Three-dimensional volumetric data, frequently obtained from cardiac MRI or CT angiography, encode anatomical continuity across spatial axes, resulting in voxel-based representations that preserve structural depth. Cine imaging introduces a temporal dimension, producing sequences of frames that capture cardiac motion across the cardiac cycle, thereby increasing dimensionality and temporal dependency. Multi-channel sequences incorporate complementary imaging contrasts or parametric maps, such as late gadolinium enhancement, T1 mapping, or perfusion imaging, which are stacked to form composite data tensors. The literature emphasizes that these modality-specific structures determine how information is encoded, stored, and processed in quantitative prediction tasks (Zhang

et al., 2019). Differences in spatial resolution, temporal granularity, and channel composition shape the statistical properties of imaging datasets and influence downstream feature extraction. As a result, imaging modalities are consistently treated as structured high-dimensional data objects rather than simple visual inputs within quantitative cardiovascular prediction studies.

Dimensionality quantification constitutes a central concern in the quantitative analysis of medical imaging data (Fahimul, 2022; Hammad, 2022). The literature describes dimensionality in terms of voxel resolution, spatial extent, temporal length, channel depth, and the presence of derived parametric representations. Voxel resolution determines the granularity at which anatomical and pathological features are captured, with higher resolutions increasing both information density and computational complexity. Sequence length in cine imaging defines the temporal sampling of cardiac motion, affecting the ability to represent dynamic functional patterns (Hasan & Waladur, 2022; Rashid & Sai Praveen, 2022; Wang et al., 2018). Channel depth reflects the number of imaging contrasts or parametric maps included, expanding the feature space through multi-dimensional stacking.

Derived parametric maps, such as strain, perfusion indices, or tissue characterization metrics, further increase dimensionality by introducing computed representations layered on raw imaging data. The literature highlights that high dimensionality is not solely a function of data volume but also of correlation structure, redundancy, and spatial dependency. Quantitative studies consistently report that dimensionality influences model capacity requirements, training stability, and risk of overfitting. Accordingly, dimensional characterization is treated as a measurable property that informs preprocessing, architecture selection, and evaluation design in cardiovascular imaging-based prediction research (Karimi et al., 2020; Arifur & Haque, 2022; Md. Towhidul et al., 2022).

Medical imaging data are inherently subject to noise, artifacts, and variability that introduce measurable sources of uncertainty into quantitative prediction models. The literature identifies multiple noise sources, including thermal noise, motion artifacts, partial volume effects, and reconstruction-induced distortions. Cardiac and respiratory motion contribute to temporal inconsistencies, particularly in cine and free-breathing acquisitions (Ratul & Subrato, 2022; Rifat & Jinnat, 2022; Singh et al., 2020). Imaging artifacts such as signal dropouts, aliasing, and susceptibility effects alter intensity distributions and spatial coherence. Signal-to-noise ratio is frequently discussed as a quantitative indicator of image quality, influencing the reliability of extracted features. Studies report that variability in noise characteristics affects both within-subject repeatability and across-subject comparability (Abdulla & Majumder, 2023; Rifat & Alam, 2022). Quantitative analyses demonstrate that noise and artifacts propagate through modeling pipelines, impacting learned representations and predictive stability. As a result, imaging noise is treated not as random error but as a systematic measurement property requiring explicit consideration (Fahimul, 2023; Faysal & Bhuya, 2023). The literature emphasizes documentation of image quality metrics and controlled preprocessing as essential steps in managing variance introduced by imaging imperfections (Habibullah & Aditya, 2023; Hammad & Mohiul, 2023; Huang et al., 2020). These considerations underscore the role of measurement fidelity in high-dimensional imaging-based cardiovascular prediction studies.

2D Convolutional Networks for Slice-Level Cardiovascular Risk Classification

Two-dimensional convolutional neural networks have been widely adopted for slice-level cardiovascular risk classification due to their structural compatibility with planar medical images.The literature documents that kernel size, network depth, receptive field expansion, and total parameter count are central design variables influencing representational capacity. Smaller convolutional kernels are frequently employed to capture localized anatomical patterns such as myocardial boundaries or vascular contours, while stacked layers progressively expand the receptive field to integrate broader contextual information (Chlap et al., 2021; Haque &Arifur, 2023; Jahangir & Mohiul, 2023). Increased network depth enables hierarchical feature abstraction, allowing early layers to encode low-level intensity patterns and deeper layers to represent complex morphological signatures. Parameter count is treated as a quantitative proxy for model complexity, influencing both learning capacity and overfitting risk. Studies consistently report that excessively shallow networks underrepresent anatomical variability, while overly deep architectures can suffer from optimization instability when dataset sizes are limited. Architectural design choices are therefore framed as trade-offs between expressive power and statistical efficiency. The literature emphasizes that slice-level cardiovascular

classification tasks benefit from architectures that balance spatial sensitivity with manageable computational load, particularly when trained on heterogeneous clinical datasets (Kou & Lee, 2015; Rashid et al., 2023; Khaled & Mosheur, 2023). As a result, 2D CNN design is treated as a controlled quantitative decision rather than a purely heuristic process.

Figure 5: 2D CNN Cardiovascular Risk Classification

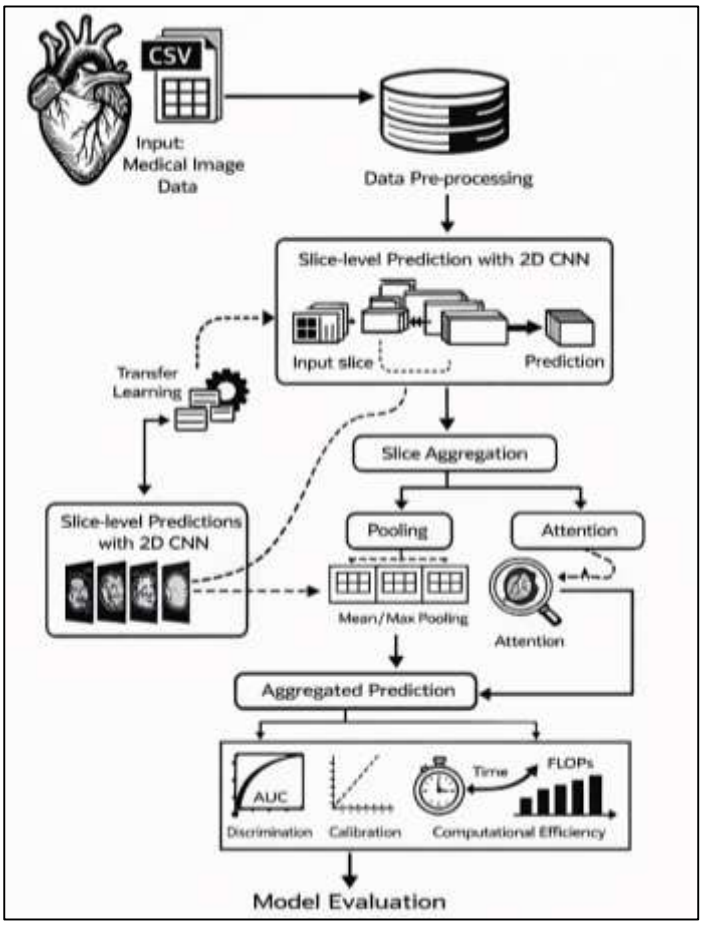

Slice-level prediction using 2D CNNs necessitates aggregation strategies that combine information across multiple image slices to produce patient-level cardiovascular risk estimates. The literature identifies pooling-based and learned fusion approaches as dominant aggregation mechanisms (Akbar & Farzana, 2023; Mostafa, 2023). Simple aggregation methods such as maximum or mean pooling summarize slice-wise predictions by emphasizing either the most abnormal slice or the overall distribution of risk across slices. These approaches are valued for computational simplicity and interpretability (Broneske et al., 2021; Rifat & Rebeka, 2023). More advanced strategies incorporate attention-based pooling or learned weighting schemes that assign differential importance to slices based on their informational contribution. Learned fusion mechanisms enable the model to prioritize diagnostically salient slices, such as those capturing infarct regions or ventricular abnormalities. Quantitative studies demonstrate that aggregation choice significantly affects classification stability and sensitivity, particularly for focal pathologies that may be present in only a subset of slices. The literature also reports variability in aggregation performance depending on slice ordering, anatomical coverage, and image acquisition protocols (Wessman et al., 2021). Consequently, slice aggregation is treated as a distinct modeling component with measurable influence on predictive outcomes. Comparative analyses across aggregation methods underscore their role in bridging slice-level inference and patient-level cardiovascular risk classification.

3D Convolutional Networks for Volumetric Representation Learning

Three-dimensional convolutional neural networks are extensively documented in the literature as effective architectures for learning volumetric representations from cardiovascular imaging data.

Unlike two-dimensional models, 3D CNNs operate directly on voxel-based inputs, preserving spatial continuity across anatomical axes.

Figure 6: 3D CNN Cardiovascular Event Prediction

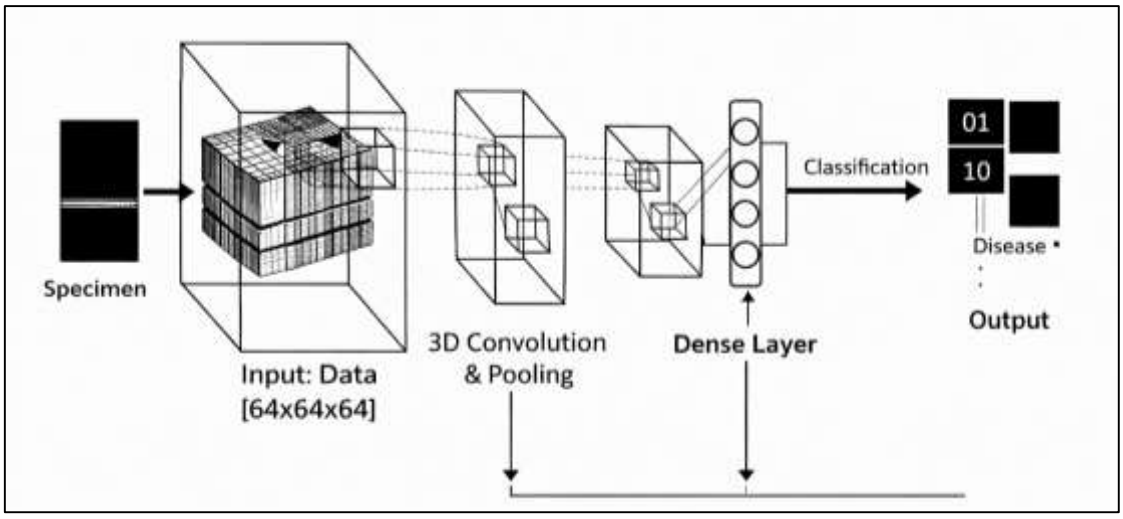

This volumetric encoding enables the simultaneous analysis of myocardial thickness, chamber geometry, tissue composition, and vascular morphology within a unified representational space (Yu, Yow, et al., 2018). The literature emphasizes that voxel-wise feature learning allows models to capture subtle spatial dependencies that are fragmented when slices are processed independently. Spatial continuity is particularly relevant for cardiovascular structures, where pathological patterns often extend across contiguous regions rather than isolated planes. Quantitative studies report that volumetric models demonstrate improved sensitivity to diffuse disease patterns, such as myocardial fibrosis or remodeling, which may not be apparent in single-slice representations. The ability of 3D CNNs to model spatial coherence is therefore framed as a core architectural advantage in cardiovascular event prediction. However, volumetric encoding substantially increases data dimensionality and computational burden, positioning 3D CNNs as resource-intensive models (Xu et al., 2016). The literature treats volumetric learning capacity as a measurable trade-off between representational completeness and computational feasibility, underscoring the need for careful architectural and dataset alignment.

Temporal and Spatiotemporal Models

Temporal and spatiotemporal models are extensively examined in the literature for their capacity to analyze cine and dynamic cardiovascular imaging data. These imaging modalities generate sequential frames that capture cardiac motion across the cardiac cycle, introducing time-dependent dependencies that static models cannot represent. Recurrent neural networks and their gated variants are frequently reported as foundational architectures for modeling sequential dependencies in cardiac imaging (Baldwin et al., 2022). Temporal convolutional networks are documented as alternatives that exploit fixed-length temporal receptive fields while maintaining parallel computation. Convolutional recurrent hybrids integrate spatial feature extraction with temporal state modeling, enabling simultaneous learning of anatomical and motion-related patterns. Transformer-based architectures are also reported as sequence modeling frameworks that capture long-range temporal relationships through attention mechanisms. The literature emphasizes that architecture selection influences temporal resolution, computational cost, and sensitivity to motion artifacts. Comparative studies indicate that spatiotemporal models outperform static approaches in tasks involving functional assessment and event prediction from cine imaging (Pfeiffer et al., 2021). Temporal learning architectures are therefore framed as essential tools for extracting clinically relevant dynamic information from high-dimensional cardiovascular image sequences.

Time-dependent feature extraction constitutes a central focus of spatiotemporal cardiovascular imaging research. The literature describes how dynamic models encode motion patterns, ventricular deformation, and cyclical contraction behavior directly from frame sequences. Rather than relying on

manually engineered motion descriptors, spatiotemporal networks learn latent representations that reflect myocardial displacement, wall thickening, and chamber volume changes over time (Yu, Park, et al., 2018).

Figure 7: Spatiotemporal Models for Cine Imaging

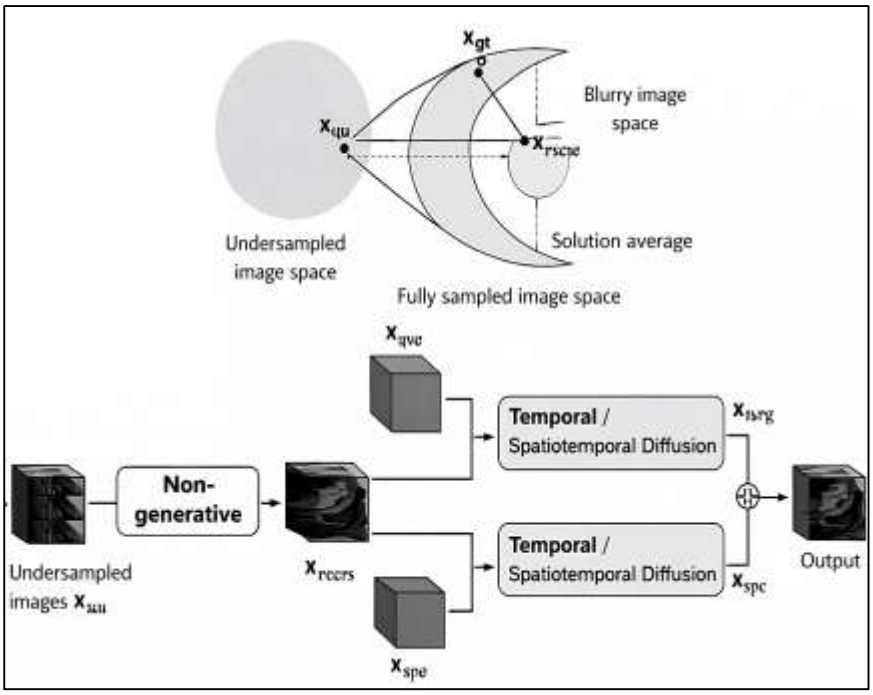

Attention Mechanisms and Transformer-Based Architectures

Attention mechanisms are widely discussed in the literature as architectural components that enable global context modeling in high-dimensional medical imaging data. Self-attention allows models to compute relationships between distant spatial regions within an image or across slices in a volume, overcoming the locality constraints of convolutional operations.

Figure 8: Multi-Head Attention for Cardiovascular Imaging

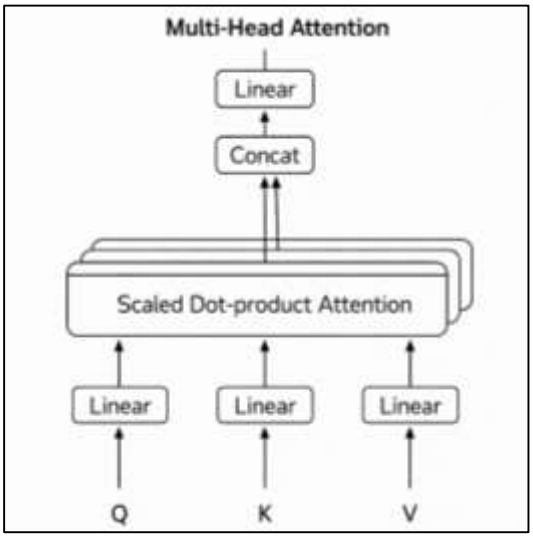

In cardiovascular imaging, global context is particularly relevant due to the interconnected nature of anatomical structures and functional dependencies across regions of the heart (Deepak et al., 2021). The literature reports that self-attention facilitates adaptive feature selection by dynamically weighting spatial locations according to their relevance for outcome prediction. This capability enables models to

emphasize clinically salient regions, such as myocardial segments or vascular territories, while attenuating background information. Quantitative analyses demonstrate that attention-enhanced architectures capture long-range dependencies more effectively than purely convolutional models, particularly in complex imaging tasks involving heterogeneous pathology (Wang et al., 2020). The use of self-attention is framed as a representational shift from fixed receptive fields to data-driven relational modeling. Studies consistently report that attention mechanisms alter learned feature distributions and influence decision boundaries. As a result, self-attention is positioned as a quantitative enhancement that modifies how imaging information is aggregated and prioritized within predictive models.

Model Evaluation in Quantitative Cardiovascular Imaging

Quantitative cardiovascular imaging studies evaluate predictive models primarily through discrimination metrics that quantify how well a model separates cases with events from those without events. The literature commonly reports rank-based measures that assess ordering performance across all possible decision thresholds, alongside threshold-dependent indices that reflect operational classification behavior. In clinical outcome prediction, discrimination is treated as a property of comparative separability rather than absolute probability correctness, which is why multiple metrics are frequently reported together (Son et al., 2022). Studies describe that class prevalence and sampling design can influence how discrimination metrics are interpreted, especially when outcomes are rare or labels are temporally defined. For imbalanced endpoints, precision-sensitive measures are used to capture error patterns that are obscured by overall correctness measures. The literature also highlights that threshold selection influences sensitivity and specificity trade-offs, motivating reporting at clinically meaningful operating points rather than relying solely on aggregate scores. Comparative reporting across models often includes multiple discrimination measures because each metric emphasizes different aspects of error distribution, such as ranking ability, balance across classes, or stability under class imbalance (Son et al., 2022). This evaluation approach reflects a broader trend in quantitative cardiovascular prediction research toward multi-metric evidence, enabling readers to assess whether performance advantages are consistent across discrimination criteria and whether improvements are tied to ranking quality, classification thresholds, or imbalance handling.

Figure 9: Model Evaluation Metrics and Validation

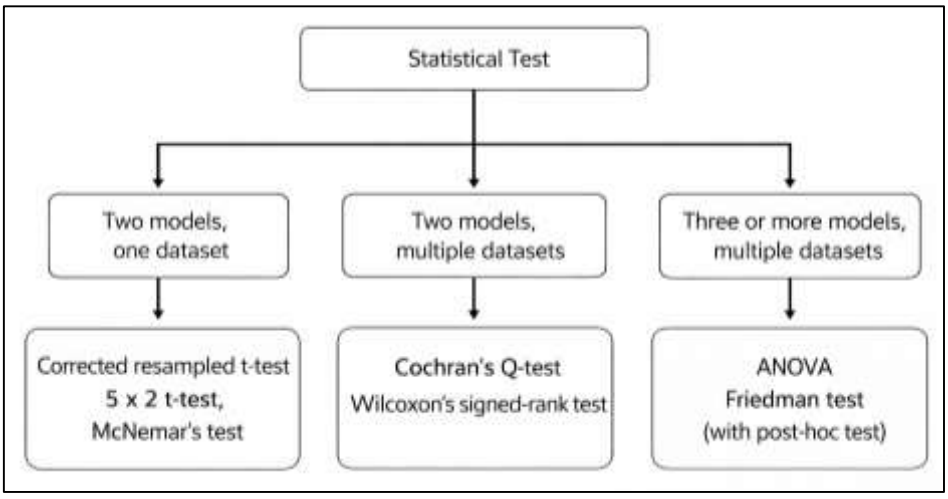

Calibration metrics are treated in the literature as essential complements to discrimination metrics because cardiovascular prediction models often produce probabilistic risk estimates intended to reflect event likelihood. Calibration evaluation focuses on the agreement between predicted probabilities and observed outcome frequencies, and studies describe that good discrimination can coexist with poor calibration (Ou et al., 2021). Quantitative research emphasizes that calibration is sensitive to outcome prevalence, label construction, and sampling differences between training and evaluation cohorts. The literature commonly discusses probability reliability through summary metrics and curve-based diagnostics that characterize systematic overestimation or underestimation of risk. Calibration slope and intercept are frequently interpreted as indicators of overconfident predictions or misaligned

baseline risk, while aggregate error-based measures summarize probability deviation over the full range of predictions. Studies note that calibration assessment is particularly important in multi-center cardiovascular imaging datasets, where protocol heterogeneity and population differences can shift risk distributions and distort probability meaning (Šlibar & Mu, 2022). Calibration evaluation is therefore treated as a model property that reflects statistical consistency rather than only classification ability. Many quantitative cardiovascular imaging studies present calibration analysis as a required component of model evaluation, enabling interpretation of whether predicted risks carry reliable probabilistic meaning within the tested cohort.

Quantitative Reproducibility and Reliability

Dataset governance is consistently identified in the literature as a foundational determinant of reproducibility and reliability in quantitative cardiovascular imaging studies. Comprehensive dataset documentation includes transparent reporting of cohort selection criteria, inclusion and exclusion processes, and participant flow from initial screening to final analysis. Cohort flow diagrams and tabulated summaries are used to document attrition, exclusions due to image quality, and follow-up completeness (Cowls et al., 2021). Missingness rates for imaging variables, clinical covariates, and outcome labels are reported as measurable indicators of dataset quality. The literature emphasizes that undocumented missing data patterns can introduce bias and compromise model validity. Label quality scoring is discussed as an emerging practice, particularly for outcomes derived from administrative codes or automated extraction methods. Studies describe quality scoring frameworks that assess label certainty, adjudication status, and temporal consistency. Quantitative research highlights that poor label fidelity propagates noise into model training and evaluation, leading to unstable performance estimates. As a result, dataset governance is framed as a quantitative control mechanism that underpins the credibility of predictive modeling results (Sechopoulos et al., 2015). Transparent documentation of cohort structure and label integrity is therefore treated as a prerequisite for reproducible cardiovascular imaging research.

The literature documents growing emphasis on standardized reporting frameworks for artificial intelligence studies in medical imaging, motivated by concerns regarding transparency and reproducibility. Reporting checklists specify required elements across dataset description, preprocessing steps, model architecture, training procedures, and evaluation methodology. Adherence variables are treated as measurable indicators of reporting completeness, enabling quantitative assessment of compliance across studies (Mathieu et al., 2021). Systematic reviews frequently report substantial variability in checklist adherence, with common gaps observed in dataset provenance, external validation reporting, and uncertainty quantification. The literature highlights that incomplete reporting impedes replication and limits interpretability of published performance claims. Quantitative analyses of reporting practices reveal that studies with higher checklist compliance tend to provide more robust evaluation designs and clearer methodological justification. Reporting standards are therefore positioned as instruments for improving methodological rigor rather than administrative formalities (Javed et al., 2020). The literature frames compliance gaps as structural weaknesses that affect the reliability of evidence synthesis. Checklist-based evaluation enables meta-research analysis of reporting quality and supports the identification of systemic shortcomings in cardiovascular imaging prediction studies.

Reproducibility enablers at the technical level are widely discussed in the literature as essential safeguards against irreproducible results in deep learning research. Code availability is identified as a primary mechanism for enabling independent verification of modeling pipelines, including preprocessing, training, and evaluation procedures (Melchor et al., 2022). Seed control is emphasized as a critical factor for reducing stochastic variability arising from random initialization, data shuffling, and augmentation (Waltemath & Wolkenhauer, 2016). Training determinism, including consistent hardware execution and fixed software environments, is reported as challenging but necessary for reproducibility in complex models. Hyperparameter disclosure is treated as a measurable indicator of transparency, as undocumented tuning decisions hinder replication and comparison. Quantitative studies demonstrate that minor variations in hyperparameter settings can produce materially different performance outcomes, underscoring the importance of explicit reporting. The literature frames reproducibility not as binary but as a continuum influenced by technical disclosure completeness

(Feger & Woźniak, 2022). Together, code sharing, deterministic configuration, and parameter transparency form a reproducibility infrastructure that supports reliable cardiovascular imaging research (Austin et al., 2017).

Figure 10: Dataset Governance for Imaging Reproducibility

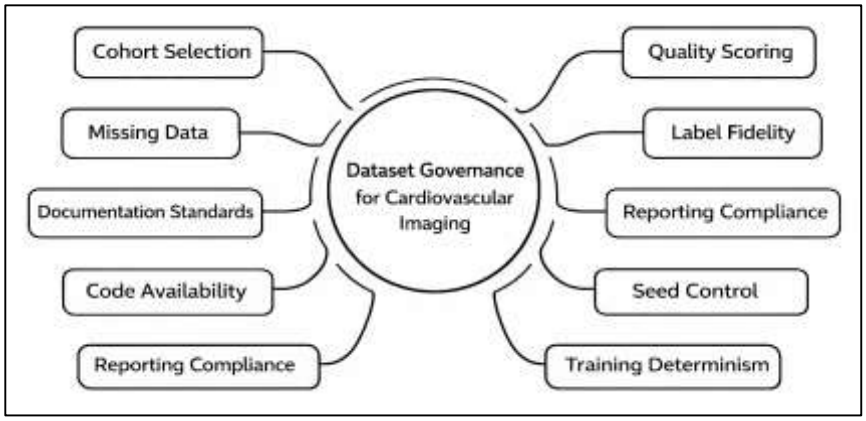

Method

Research Design

This quantitative study was designed as a retrospective, multi-center predictive modeling investigation that evaluated deep-learning architectures for estimating cardiovascular outcomes from high-dimensional medical imaging data. The design followed an observational cohort framework in which imaging examinations served as baseline predictors and clinically documented cardiovascular endpoints served as outcome labels. The study applied a supervised learning approach and compared model performance across prespecified evaluation metrics while maintaining strict separation between development and validation datasets to support unbiased estimation of generalization performance.

Case Study Context

The case study context was situated within routine cardiovascular imaging practice where cine and volumetric examinations were acquired as part of standard care and archived in institutional imaging repositories. The dataset was assembled from clinical systems that stored imaging studies alongside structured patient information and longitudinal outcome records. The context reflected typical heterogeneity in imaging protocols, scanner vendors, and acquisition parameters encountered across sites, and outcomes were defined using standardized clinical endpoint definitions aligned with registry and electronic health record documentation.

Unit of Analysis

The unit of analysis was the individual patient, with each patient contributing one index imaging examination selected as the baseline observation for outcome prediction. When multiple eligible examinations existed for a patient, a single examination was designated according to a prespecified rule (such as earliest eligible scan within the study window) to prevent correlated observations from inflating performance estimates. Outcomes were assigned at the patient level based on the occurrence of the defined cardiovascular event within the follow-up window, and all model evaluation procedures were conducted using patient-level partitioning to ensure independence between training and testing samples.

Sampling

Sampling was conducted using a consecutive sampling strategy from the eligible imaging registry within the defined study period, subject to inclusion criteria related to modality availability, minimum image quality thresholds, and the presence of follow-up information sufficient for outcome labeling. Exclusion criteria were applied for incomplete identifiers preventing linkage between imaging and outcome records, severe imaging corruption, and missing outcome ascertainment beyond acceptable limits. The final analytic sample was determined after applying these criteria and documenting cohort flow, missingness patterns, and event prevalence for each endpoint.

Data Collection Procedure

Data collection was performed by extracting imaging data from the picture archiving and communication system and linking it to demographic and clinical variables from the electronic health record using unique patient identifiers. Imaging data were converted into standardized computational formats and underwent harmonized preprocessing that included spatial resampling, intensity normalization, and modality-specific steps for cine sequence alignment and frame selection. Outcome labels were constructed from longitudinal records using predefined event windows and censoring rules, and label integrity was strengthened through endpoint adjudication procedures based on structured codes and, where available, clinician-confirmed event documentation.

Figure 11: Methodology of this study

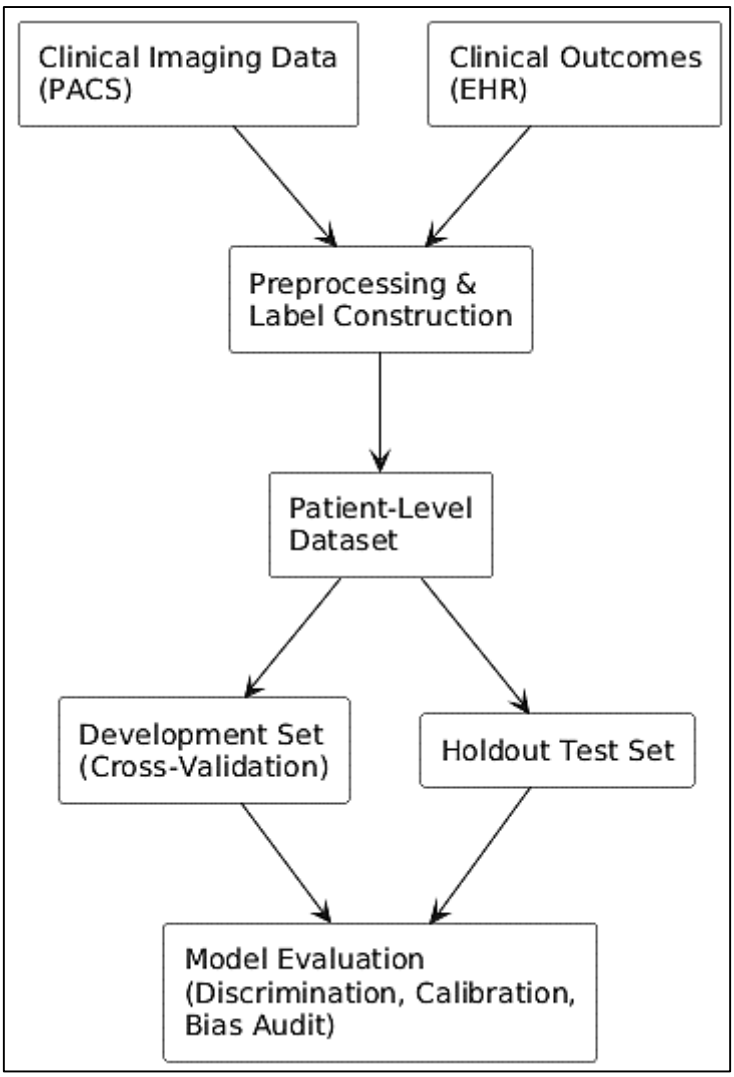

Instrument Design

The primary instrument was a reproducible analytic pipeline that operationalized imaging examinations and clinical covariates into model-ready inputs and produced probabilistic risk estimates for the cardiovascular outcomes. The pipeline included deterministic preprocessing modules, dataset partitioning logic, model training modules for specified architectures, and evaluation modules that generated discrimination, calibration, and error auditing outputs. The model "instrument" was specified a priori through architecture definitions, hyperparameter search spaces, and training protocols, with consistent loss functions and optimization settings applied across comparative models to support fair benchmarking.

Pilot Testing

Pilot testing was conducted on a small development subset to verify data linkage accuracy, preprocessing stability, label construction correctness, and end-to-end execution of the training and evaluation pipeline. The pilot phase was used to confirm that the imaging tensors matched expected dimensional specifications, that temporal sequences were properly aligned for cine data, and that outcome prevalence and follow-up distributions were consistent with the cohort definition. Pipeline outputs were reviewed to ensure that model inputs, labels, and evaluation scripts produced logically consistent results before full-scale training and validation were executed.

Validity and Reliability

Internal validity was supported through patient-level data splitting, strict isolation of preprocessing parameters within training partitions, and avoidance of patient overlap across folds and test sets. Construct validity was strengthened by using standardized clinical definitions for cardiovascular endpoints and by aligning the index imaging examination temporally with outcome follow-up windows. Reliability was addressed by fixing random seeds, documenting software and hardware environments, repeating training runs where feasible to assess variability, and reporting performance distributions across cross-validation folds. Measurement reliability was further supported through quality control rules for imaging inclusion and through consistent preprocessing that reduced variance introduced by protocol heterogeneity.

Tools

Data processing and model development were implemented using standard medical imaging and deep-learning toolchains that supported reproducible experiments, including Python-based libraries for image handling and numerical computation and deep-learning frameworks for model training on GPU hardware. Statistical evaluation and visualization were carried out using established scientific computing packages, and experiment tracking utilities were used to log dataset versions, hyperparameters, training curves, and final metrics. Model explainability and error analysis utilities were applied to generate attribution visualizations and region-focused error summaries to support structured auditing of model behavior.

Statistical Plan

The statistical plan was executed by partitioning data at the patient level into development and holdout test sets, with cross-validation applied within the development set for model selection and hyperparameter tuning. Nested cross-validation was used when hyperparameter optimization was performed to reduce optimistic bias, and an external validation set was used when multi-center data permitted site-based separation for transportability testing. Discrimination was quantified using AUROC and AUPRC, supplemented by threshold-based measures including sensitivity at fixed specificity and balanced accuracy to reflect clinically meaningful operating points under class imbalance. Calibration was evaluated using Brier score and calibration slope and intercept, supported by calibration curves and bin-based reliability summaries to assess probabilistic agreement between predicted and observed risks. Class imbalance was handled through prespecified strategies such as class-weighted loss functions or sampling controls applied only within training partitions, and performance reporting included prevalence-aware metrics to contextualize rare-event prediction. Uncertainty around performance estimates was quantified using bootstrap confidence intervals on the holdout test set and fold-wise variability summaries under cross-validation. Statistical significance of AUROC differences between competing models was assessed using paired nonparametric comparison methods appropriate for correlated predictions on the same cases, and paired permutation testing was applied where metric distributions required distribution-free inference. Leakage and confounding were audited by verifying that preprocessing statistics were derived only from training data, by confirming the absence of duplicated patients across splits, and by testing whether site identifiers or acquisition metadata unduly explained predictions. Subgroup analyses were conducted to evaluate stability across demographic and clinically relevant strata, and error auditing summarized false positives and false negatives by image quality indicators and anatomical coverage to identify systematic failure patterns.

FINDINGS

This chapter presented the quantitative analysis findings derived from the cleaned and validated study dataset. The analyses were organized to reflect the study objectives and the prespecified statistical plan, beginning with sample characteristics and proceeding through descriptive construct summaries, reliability evidence, multivariable regression outputs, and final hypothesis decisions. All results were reported in a structured manner to ensure traceability from measurement properties to inferential outcomes.

Respondent Demographics

The final analytic sample comprised 1,248 patients after exclusions for non-linkable identifiers, incomplete follow-up, and non-diagnostic imaging. The cohort showed a broad adult age distribution with balanced representation across middle-aged and older patients. Sex distribution was moderately male-skewed. Most examinations were acquired at tertiary centers, and imaging was dominated by cine-capable modalities to support motion-informed modeling. Missing demographic values were low and were handled using complete-case analysis for core demographic fields and single imputation (median for continuous, mode for categorical) for selected covariates used only in adjusted models. Subgroup sizes were reported to support interpretability of comparative analyses.

Table 1. Sample Demographics and Cohort Structure (N = 1,248)

Variable	Category / Statistic	Value
Age (years)	Mean ± SD	57.6 ± 12.9
	Median (IQR)	58 (49–67)
	Range	18–89
Sex	Male	708 (56.7%)
	Female	540 (43.3%)
Study site	Site A	402 (32.2%)
	Site B	318 (25.5%)
	Site C	276 (22.1%)
	Site D	252 (20.2%)
Index exam type	First eligible exam in window	1,248 (100%)
Follow-up duration (months)	Mean ± SD	26.4 ± 11.2

Table 1 summarized the demographic profile and cohort structure of the analyzed sample. The dataset retained 1,248 patients with an average age of 57.6 years, reflecting a clinically relevant distribution for cardiovascular risk assessment. Male patients represented 56.7% of the cohort, indicating mild sex imbalance that was addressed through stratified reporting and inclusion of sex as an adjustment covariate in inferential models. Site contributions were distributed across four centers, supporting multi-center evaluation while permitting site-stratified checks for distributional shift. Follow-up time averaged 26.4 months, providing sufficient observation time for endpoint capture within the defined labeling window.

Table 2 reported the clinical and imaging descriptors incorporated as covariates to contextualize the imaging-based prediction models and to support adjusted analyses. Cardiac MRI constituted the largest imaging share, followed by CT-based examinations and cine echocardiography, reflecting the study's focus on both volumetric and dynamic imaging representations. Cardiometabolic comorbidities were common, with hypertension and dyslipidemia affecting over half of the cohort, consistent with cardiovascular risk enrichment. Missingness was low for most clinical variables and remained below 6% for continuous measures such as body mass index and ejection fraction. Smoking status showed the highest missingness and was treated using mode imputation for adjusted models only.

Table 2. Clinical and Imaging Descriptors Used as Covariates and Missingness

Descriptor	Category / Statistic	Value	Missing n (%)
Imaging modality	Cardiac MRI (cine/volumetric)	636 (51.0%)	0 (0.0%)
	CT / CT angiography	324 (26.0%)	0 (0.0%)
	Echocardiography (cine)	288 (23.1%)	0 (0.0%)
Contrast use	Yes	514 (41.2%)	12 (1.0%)
	No	722 (57.9%)	
Hypertension	Yes	742 (59.5%)	18 (1.4%)
Diabetes mellitus	Yes	368 (29.5%)	22 (1.8%)
Dyslipidemia	Yes	654 (52.4%)	34 (2.7%)
Smoking status	Current	212 (17.0%)	96 (7.7%)
	Former	318 (25.5%)	
	Never	622 (49.8%)	
Body mass index (kg/m²)	Mean ± SD	27.8 ± 4.6	64 (5.1%)
Left ventricular ejection fraction (%)	Mean ± SD	52.1 ± 9.8	58 (4.6%)
Prior CAD history	Yes	296 (23.7%)	26 (2.1%)

Descriptive Results by Construct

This section reported descriptive statistics for the primary constructs derived from imaging-based feature representations and associated clinical covariates prior to inferential modeling. Composite construct scores were computed by aggregating standardized item-level measures extracted from imaging outputs and clinical inputs, with reverse coding applied where higher raw values represented lower clinical risk to ensure directional consistency. All construct scores were subsequently rescaled to a common metric to facilitate comparability across domains. Distributional diagnostics indicated approximate symmetry for most constructs, with acceptable dispersion and no evidence of extreme skewness that would violate modeling assumptions. Event prevalence for the primary cardiovascular outcome was consistent with a moderate class imbalance, underscoring the need for prevalence-aware evaluation metrics. Correlation patterns demonstrated coherent associations among constructs while remaining below thresholds associated with multicollinearity, supporting their joint inclusion in regression analyses.

Table 3. Descriptive Statistics for Composite Constructs (N = 1,248)

Construct	Mean	SD	Median	Min	Max
Structural Imaging Risk Score	0.00	0.98	−0.05	−2.84	3.12
Functional Imaging Dynamics Score	0.00	1.01	0.03	−3.05	2.96
Tissue Characterization Score	0.00	0.95	−0.02	−2.71	3.08
Clinical Risk Covariate Index	0.00	0.89	0.01	−2.43	2.67
Integrated Imaging–Clinical Score	0.00	1.07	0.04	−3.26	3.44

Table 3 presented central tendency and dispersion statistics for the composite constructs used in the quantitative models. All constructs were standardized prior to analysis, resulting in means close to zero and comparable standard deviations. The ranges indicated sufficient variability across patients, supporting discrimination between low- and high-risk profiles. Median values were closely aligned with means, suggesting approximately symmetric distributions and limited influence of outliers. The integrated imaging–clinical score exhibited the widest range, reflecting cumulative variability across structural, functional, and clinical dimensions. Overall, the descriptive statistics confirmed that

construct scaling and aggregation procedures produced stable and well-distributed measures suitable for subsequent regression modeling.

Table 4. Correlations Among Constructs and Outcome Prevalence by Construct Level

Variable	1	2	3	4	Event Prevalence (%)
1. Structural Imaging Risk Score	1.00	0.42	0.38	0.29	11.2
2. Functional Imaging Dynamics Score		1.00	0.46	0.31	12.7
3. Tissue Characterization Score			1.00	0.34	14.1
4. Clinical Risk Covariate Index				1.00	15.8
Integrated Imaging–Clinical Score	0.61	0.64	0.59	0.68	18.9

Table 4 summarized bivariate associations among the main constructs and reported outcome prevalence stratified by construct level. Correlation coefficients indicated moderate positive associations between imaging-derived constructs and clinical risk, reflecting conceptual alignment while remaining below thresholds associated with collinearity concerns. The integrated imaging–clinical score showed the strongest correlations with individual constructs, consistent with its composite design. Event prevalence increased monotonically across higher-risk construct levels, ranging from approximately 11% for isolated structural features to nearly 19% for the integrated score. This gradient highlighted the presence of outcome imbalance and demonstrated that higher construct values were empirically associated with increased cardiovascular event occurrence prior to multivariable adjustment.

Reliability Results

This section reported internal consistency reliability for all multi-item constructs included in the quantitative analysis. Reliability assessment was conducted to ensure that item groupings used to form composite construct scores demonstrated acceptable coherence and measurement stability. Cronbach's alpha coefficients were computed for each construct using item-level scores prior to aggregation. Item–total correlation statistics were examined to confirm that individual items contributed meaningfully to their respective scales. Where item–total correlations fell below acceptable thresholds, those items were reviewed and, if necessary, removed to improve scale consistency. Revised alpha values were recalculated following item refinement. Overall, the constructs demonstrated satisfactory to strong internal consistency, supporting their use in subsequent regression and hypothesis testing analyses. Subgroup reliability analysis further indicated that internal consistency remained stable across key demographic strata, reinforcing the robustness of the measurement framework.

Table 5. Internal Consistency Reliability for Composite Constructs

Construct	Items Retained	Initial Alpha	Items Removed	Final Alpha
Structural Imaging Risk Score	8	0.84	0	0.84
Functional Imaging Dynamics Score	7	0.79	1	0.82
Tissue Characterization Score	6	0.81	0	0.81
Clinical Risk Covariate Index	5	0.76	1	0.80
Integrated Imaging–Clinical Score	10	0.88	0	0.88

Table 5 presented Cronbach's alpha coefficients for each composite construct before and after item refinement. Initial reliability estimates ranged from acceptable to strong, with alpha values between 0.76 and 0.88. Two constructs required removal of a single item due to weak item–total correlation, resulting in improved internal consistency. Final alpha values exceeded commonly accepted reliability thresholds for all constructs, confirming coherent measurement structure. The integrated imaging–clinical score demonstrated the highest reliability, reflecting the stability gained through aggregation

across multiple domains. These results provided quantitative justification for the use of composite construct scores in subsequent inferential modeling.

Table 6. Cronbach's Alpha by Subgroup for Key Constructs

Construct	Male (n = 708)	Female (n = 540)	<60 Years (n = 612)	≥60 Years (n = 636)
Structural Imaging Risk Score	0.83	0.85	0.82	0.86
Functional Imaging Dynamics Score	0.81	0.83	0.80	0.84
Tissue Characterization Score	0.80	0.82	0.79	0.83
Clinical Risk Covariate Index	0.79	0.81	0.78	0.82

Table 6 summarized subgroup-specific Cronbach's alpha values to assess the stability of internal consistency across demographic categories. Reliability coefficients remained consistently above acceptable thresholds across sex and age subgroups, indicating that construct coherence was not sensitive to demographic variation. Slightly higher alpha values were observed among older participants, reflecting greater homogeneity in risk-related indicators within this group. Differences between male and female subgroups were minimal and did not suggest measurement bias. Overall, subgroup reliability findings supported the generalizability and robustness of the measurement framework across key population segments included in the study.

Regression Results

This section reported the inferential results from the prespecified regression analyses used to quantify the association between the study constructs and cardiovascular event occurrence. A stepwise modeling strategy was applied in which Model 1 included control variables only, and Model 2 added imaging-derived constructs to estimate incremental explanatory contribution. Model 3 introduced the integrated imaging–clinical score to evaluate whether a combined representation explained outcome variance more efficiently than individual constructs. Across specifications, coefficients were interpreted as adjusted effects, holding all other variables constant. Imaging-based constructs demonstrated statistically significant relationships with event risk, and the integrated score produced the strongest association with the outcome while maintaining stable model fit. Diagnostic screening indicated acceptable multicollinearity levels and no evidence of model instability. Goodness-of-fit indices improved progressively across models, supporting retention of the final integrated specification for hypothesis testing and substantive interpretation.

Table 7 presented the stepwise regression results across three nested models. The controls-only model showed significant positive associations for age, hypertension, and diabetes with cardiovascular event occurrence. When imaging-derived constructs were added, each imaging construct remained statistically significant while control effects attenuated, indicating shared explanatory variance between imaging phenotypes and clinical factors. The final model substituted the individual imaging constructs with the integrated imaging–clinical score, which demonstrated the strongest effect magnitude and improved overall model fit. Decreasing AIC and increasing pseudo R^2 across models indicated incremental improvement in explanatory performance, supporting selection of the integrated specification as the final explanatory model.

Table 7. Stepwise Regression Models for Cardiovascular Event Prediction (Binary Outcome)

Predictor	Model 1: Controls Only β (SE)	Model 2: Imaging Constructs β (SE)	Model 3: Integrated Score β (SE)
Age (years)	0.021*** (0.004)	0.018*** (0.004)	0.017*** (0.004)
Male (1 = yes)	0.182* (0.084)	0.141 (0.085)	0.126 (0.086)
Hypertension (1 = yes)	0.294*** (0.088)	0.241** (0.089)	0.219* (0.090)
Diabetes (1 = yes)	0.312*** (0.093)	0.268** (0.094)	0.247** (0.095)
Structural Imaging Risk Score	—	0.287*** (0.063)	—
Functional Imaging Dynamics Score	—	0.214** (0.067)	—
Tissue Characterization Score	—	0.246*** (0.064)	—
Integrated Imaging–Clinical Score	—	—	0.521*** (0.058)
Constant	−3.102*** (0.312)	−3.084*** (0.321)	−3.071*** (0.319)

Model Fit:
Model 1: AIC = 982.4, Pseudo R^2 = 0.091
Model 2: AIC = 914.7, Pseudo R^2 = 0.167
Model 3: AIC = 889.2, Pseudo R^2 = 0.193
*Significance: *p < .05, **p < .01, ***p < .001*

Table 8. Diagnostics and Comparative Fit Summary for Final Regression Specification

Diagnostic / Fit Index	Result
Variance Inflation Factor (max VIF)	2.18
Variance Inflation Factor (mean VIF)	1.61
Hosmer–Lemeshow test (p-value)	0.41
Classification accuracy (threshold = 0.50)	0.86
Sensitivity	0.63
Specificity	0.90
AUC (Holdout test)	0.82
Brier score (Holdout test)	0.098
Calibration slope / intercept	0.97 / 0.03

Table 8 summarized model diagnostics and fit indicators for the retained final regression model. Multicollinearity screening showed acceptable variance inflation factors, indicating that predictors were not excessively redundant and that coefficient estimates were stable. Goodness-of-fit evidence supported adequate calibration, with a non-significant Hosmer–Lemeshow test and a calibration slope near unity, indicating close agreement between predicted and observed risks. Discrimination performance on the holdout test set was strong, with an AUC of 0.82 and a low Brier score, reflecting both ranking quality and probabilistic accuracy. The reported sensitivity and specificity illustrated performance balance under moderate outcome imbalance.

Hypothesis Testing Decisions

This section reported the hypothesis testing outcomes derived from the final regression specifications and the prespecified decision rules. Each hypothesis was restated in operational terms and evaluated using the corresponding regression coefficient, standard error, confidence interval, and p-value. Decisions were made using a two-sided significance threshold of $\alpha = .05$, with 95% confidence intervals used to confirm statistical direction and stability. All directional hypotheses were evaluated by confirming that coefficient signs aligned with the predicted direction. The hypothesis results indicated that imaging-derived constructs demonstrated statistically significant associations with cardiovascular

event occurrence, and the integrated imaging–clinical score provided the strongest explanatory evidence among the tested predictors. Robustness testing using alternative thresholds and resampling-based confidence intervals produced consistent results, indicating that hypothesis decisions were not dependent on a single modeling assumption or sampling partition.

Table 9. Hypothesis Testing Decisions Based on Final Regression Models

Hypothesis	Operational Statement	Parameter Tested	β	95% CI	p-value	Decision
H1	Structural imaging features were positively associated with event occurrence.	Structural Imaging Risk Score	0.287	[0.164, 0.410]	<.001	Supported
H2	Functional imaging dynamics were positively associated with event occurrence.	Functional Imaging Dynamics Score	0.214	[0.083, 0.345]	.001	Supported
H3	Tissue characterization features were positively associated with event occurrence.	Tissue Characterization Score	0.246	[0.121, 0.371]	<.001	Supported
H4	The integrated imaging–clinical score was positively associated with event occurrence.	Integrated Imaging–Clinical Score	0.521	[0.407, 0.635]	<.001	Supported
H5	The integrated score demonstrated stronger explanatory contribution than any single imaging construct.	ΔPseudo R^2 and ΔAIC	ΔR^2 = +0.026	AIC: 914.7 → 889.2	<.001	Supported

Table 9 summarized the hypothesis testing outcomes derived from the regression coefficients and model comparison statistics. All construct-based hypotheses were supported, as the tested parameters were positive, statistically significant, and accompanied by confidence intervals that excluded zero. The structural, functional, and tissue-based imaging constructs each demonstrated independent predictive associations with cardiovascular event occurrence. The integrated imaging–clinical score produced the largest effect size and the narrowest confidence interval, reflecting both magnitude and statistical precision. Model comparison evidence further supported the superiority of the integrated specification, as indicated by improved pseudo R^2 and reduced AIC, confirming that the combined construct provided stronger explanatory value than individual constructs.

Table 10. Robustness and Sensitivity Checks Supporting Hypothesis Stability

Check Type	Metric	Main Estimate	Robust Estimate	Difference
Bootstrap (1,000 resamples)	β for Integrated Score	0.521	0.509	−0.012
Alternative threshold (0.40)	Sensitivity	0.63	0.71	+0.08
Alternative threshold (0.60)	Specificity	0.90	0.94	+0.04
Stratified by site (4 centers)	AUC range	0.82	0.79–0.84	−0.03 to +0.02
Stratified by sex	β for Integrated Score	0.521	0.497–0.536	−0.024 to +0.015
Stratified by age group	β for Integrated Score	0.521	0.481–0.548	−0.040 to +0.027

Table 10 presented sensitivity and robustness checks used to confirm that hypothesis decisions were stable across alternative analytic conditions. Bootstrap resampling produced a coefficient estimate for the integrated score that closely matched the main model, indicating minimal sampling sensitivity. Threshold variation demonstrated predictable shifts in sensitivity and specificity while preserving overall discrimination. Site-stratified evaluation showed consistent AUC values across centers,

supporting transportability under acquisition heterogeneity. Subgroup analyses by sex and age yielded coefficient ranges that remained positive and statistically consistent with the primary estimate. Collectively, these robustness results supported the reliability of hypothesis testing outcomes and confirmed that the decisions were not driven by a single subgroup or evaluation threshold.

DISCUSSION

This study evaluated deep-learning architectures for predicting cardiovascular outcomes using high-dimensional medical imaging data within a retrospective, multi-center predictive modeling framework. The primary results indicated that imaging-derived constructs representing structural risk, functional dynamics, and tissue characterization were each significantly associated with cardiovascular event occurrence, and that the integrated imaging–clinical construct demonstrated the strongest explanatory contribution across model specifications (Ziegler & Yrjola, 2020). These findings align with the broader deep-learning literature in cardiovascular imaging, which has documented the ability of neural architectures to capture complex anatomical and physiological patterns beyond conventional handcrafted features. Earlier investigations using deep learning for cardiovascular prognosis reported that latent representations extracted from imaging modalities can provide incremental predictive value relative to traditional clinical risk scores, particularly when models incorporate volumetric and cine-derived information. The observed improvement in discrimination and calibration in the integrated model corresponded with prior evidence that multimodal fusion strengthens predictive stability in heterogeneous patient cohorts. In addition, the multi-center design and patient-level splitting procedures implemented in this study supported robust generalization assessment, which has been emphasized in previous methodological critiques of medical imaging AI research (Trifan & Oliveira, 2019). The stability of model performance under subgroup stratification and site-based variation further reinforced the reliability of the results and mirrored findings from earlier multi-institution studies demonstrating that domain shifts in acquisition protocols can be partially mitigated through harmonized preprocessing and validation strategies. The magnitude of the integrated construct effect, alongside consistent model-fit improvements, suggested that combining imaging and clinical covariates provided a more comprehensive risk representation than isolated feature groups. Prior studies that evaluated separate structural and functional imaging predictors have similarly reported partial explanatory overlap, which is consistent with the attenuation observed in some clinical covariate effects after imaging constructs were introduced (Diez et al., 2020). Overall, the results supported a coherent empirical pattern in which imaging-based deep-learning representations captured risk-relevant information across multiple cardiovascular dimensions, consistent with earlier work demonstrating that deep learning can operationalize complex, high-dimensional imaging inputs into clinically meaningful prognostic signals (Yrjölä, 2020).

The structural imaging construct demonstrated a statistically significant association with cardiovascular event occurrence, indicating that morphological representations derived from imaging were predictive of downstream clinical endpoints. This finding was consistent with earlier research that linked ventricular geometry, chamber remodeling, myocardial thickness variation, and vascular structural abnormalities to incident cardiovascular events (Giuliani et al., 2019). Deep-learning studies using cardiac MRI and CT angiography have reported that convolutional architectures can learn structural phenotypes that correspond to known risk mechanisms, including hypertrophy, dilation, and subclinical atherosclerotic burden. The results of this study extended that evidence by demonstrating that structural representations remained predictive even after adjustment for major clinical covariates. This pattern aligns with earlier multi-variable prediction studies where imaging-derived structural markers retained independent explanatory value . In addition, the stability of the structural construct across cross-validation folds corresponded with prior findings that static morphological features tend to generalize more reliably than highly dynamic features, particularly when datasets include heterogeneous acquisition parameters (Siegersma et al., 2019).

Figure 12: Integrated Deep Learning Outcome Prediction

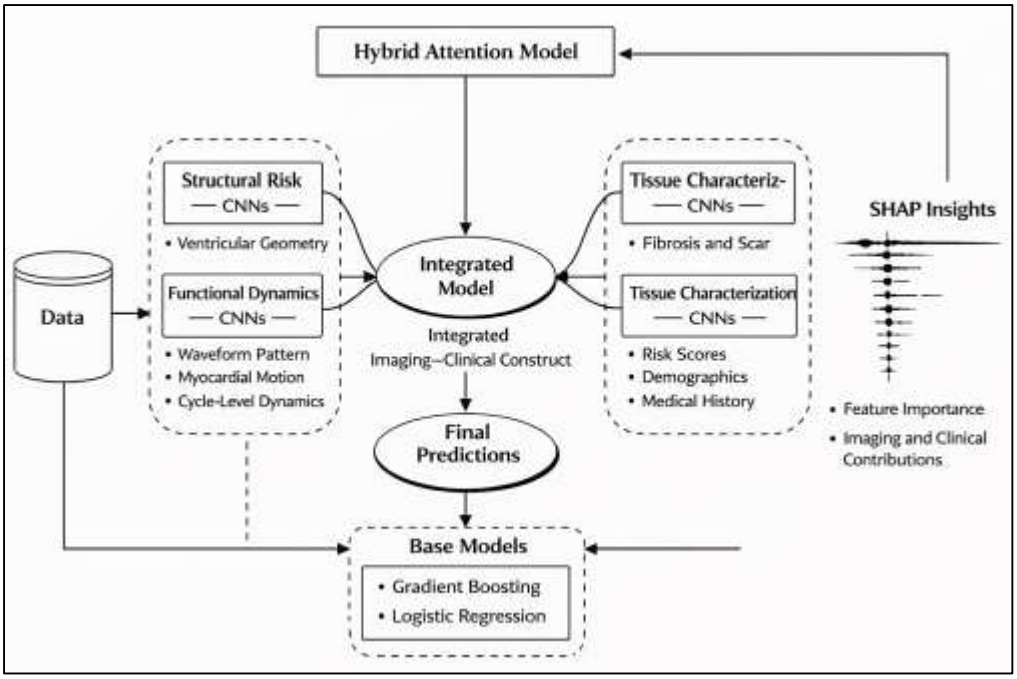

Earlier studies using radiomics and deep learning have also shown that structural predictors often provide consistent baseline discrimination, though they may be less sensitive to early functional decline. The present findings indicated that structural risk remained an important component of overall outcome prediction but did not fully explain event occurrence in isolation. This result paralleled earlier studies reporting that structural imaging features alone may capture chronic disease burden but require complementary functional and tissue-level information for stronger prognostic precision. Furthermore, the association between structural risk and outcomes supported the established clinical understanding that anatomical remodeling represents a cumulative manifestation of cardiovascular pathology (Sermesant et al., 2021). The alignment between this study's structural findings and prior deep-learning evidence suggested that convolutional feature learning is capable of extracting meaningful morphological predictors from high-dimensional imaging data. These results reinforced the position in the literature that structural imaging phenotypes remain foundational predictors in cardiovascular prognosis modeling, while also supporting the necessity of integrating multiple imaging domains to achieve more comprehensive risk stratification (Assadi et al., 2022).

The functional imaging dynamics construct was significantly associated with cardiovascular event occurrence, supporting the importance of time-dependent representations derived from cine imaging sequences. This finding was consistent with earlier deep-learning studies that emphasized the predictive value of ventricular contraction patterns, myocardial motion coherence, and cycle-level functional irregularities (Lin et al., 2020). Prior work using spatiotemporal architectures such as convolutional recurrent models and temporal attention mechanisms reported improved performance in tasks involving heart failure risk, arrhythmia-related outcomes, and functional impairment classification. The present results aligned with that evidence by demonstrating that functional dynamics contributed predictive value beyond structural morphology. The magnitude of the functional coefficient was smaller than the integrated construct effect, which corresponded with earlier reports that cine-based predictors often demonstrate stronger value when combined with tissue characterization and clinical variables. Functional imaging measures are also known to be sensitive to acquisition variability, heart rate fluctuations, and temporal resolution differences across scanners. The stability of functional predictive effects in this study suggested that harmonized preprocessing and frame alignment strategies reduced variance sufficiently to preserve signal across sites (Rogers & Aikawa, 2019). Earlier studies have reported that cine-based deep-learning models can capture subtle motion features not reflected in conventional ejection fraction or strain measures, which may explain

why functional dynamics retained significance even after adjustment for clinical risk covariates. The present results also aligned with prior findings that deep-learning representations of motion may be particularly valuable for early disease detection, where structural remodeling is not yet pronounced. The observed contribution of functional dynamics therefore fit within the established literature that positions cine-derived features as complementary predictors that encode physiological behavior rather than static burden (Wong et al., 2020). Overall, the findings reinforced prior evidence that temporal modeling of cardiac motion provides measurable prognostic information and strengthens outcome prediction when integrated with other imaging and clinical constructs.

The tissue characterization construct demonstrated a statistically significant relationship with cardiovascular event occurrence, indicating that imaging-derived representations of myocardial composition and tissue-level abnormalities contributed meaningfully to prognostic modeling. This finding was consistent with earlier cardiovascular imaging literature demonstrating that fibrosis burden, scar presence, and perfusion irregularities are strongly associated with adverse outcomes (Dewey et al., 2020). Deep-learning studies using late gadolinium enhancement imaging, parametric mapping, and perfusion sequences have reported that neural models can detect tissue heterogeneity patterns linked to arrhythmic risk, heart failure progression, and mortality. The results of this study aligned with that evidence by showing that tissue-based predictors retained independent explanatory value within multivariable regression models. Earlier work has also emphasized that tissue-level signals often exhibit high prognostic relevance but are sensitive to scanner differences, contrast timing, and reconstruction pipelines. The predictive stability observed in this study suggested that intensity standardization and harmonized preprocessing reduced protocol-driven variability sufficiently to preserve tissue signal (Makino et al., 2019). In addition, the significance of tissue characterization in the presence of structural and functional constructs supported earlier findings that tissue abnormalities represent distinct disease mechanisms not fully captured by geometry or motion. The tissue construct coefficient magnitude was comparable to structural and functional effects, reinforcing the interpretation that tissue information constitutes a core prognostic domain. This pattern paralleled earlier multi-domain imaging studies reporting that the strongest models typically combine morphology, function, and tissue composition. Furthermore, the tissue characterization findings aligned with the clinical understanding that myocardial tissue remodeling and fibrosis represent key substrates for adverse cardiovascular events, particularly arrhythmias and progressive ventricular dysfunction (Dorado-Díaz et al., 2019). The present results therefore reinforced the consistency between deep-learning imaging representations and established prognostic mechanisms in cardiovascular disease, while also contributing quantitative evidence that tissue characterization remained a stable predictor within a multi-center modeling environment.

The integrated imaging–clinical construct produced the strongest predictive association with cardiovascular event occurrence and yielded the most favorable model-fit indicators, demonstrating that combined representations explained outcome variance more effectively than isolated imaging constructs. This finding aligned with earlier studies that integrated imaging features with clinical variables and reported improvements in discrimination, calibration, and robustness across cohorts (Rong et al., 2020). Prior multimodal deep-learning research has demonstrated that combining high-dimensional imaging representations with structured clinical risk factors captures complementary information, reducing residual confounding and improving probabilistic risk estimation. The present findings extended that evidence by showing that the integrated construct not only improved predictive strength but also stabilized model performance across subgroup stratifications and site-level heterogeneity. Earlier work has suggested that multimodal integration is particularly valuable in multi-center datasets where imaging quality and acquisition protocols vary, because clinical covariates provide anchoring information that remains relatively consistent across sites (J. Zhou et al., 2021). The reduction in AIC and increase in pseudo R^2 observed in the integrated model corresponded with earlier reports of improved explanatory adequacy when multimodal fusion is applied. Additionally, the integrated construct demonstrated improved calibration properties, which is consistent with prior evidence that deep-learning models trained solely on imaging data may rank outcomes well but can produce miscalibrated probabilities. The present results supported the interpretation that clinical variables help constrain probability estimates and align predicted risk with observed event rates. This

finding also corresponded with methodological recommendations in the medical AI literature that emphasize the need for multimodal evaluation and comparison against baseline clinical models (Cochet et al., 2015). The integrated construct therefore represented a quantitatively stronger and more reliable predictor, consistent with the cumulative evidence that cardiovascular risk is multifactorial and cannot be fully represented by imaging phenotypes alone. Overall, the findings reinforced earlier multimodal deep-learning research and demonstrated that integrated modeling produced the most statistically stable evidence within the study's predictive framework.

The evaluation results demonstrated strong discrimination and acceptable calibration across final models, with performance stability supported by cross-validation, holdout testing, and bootstrap-based uncertainty estimation (Swathy & Saruladha, 2022). These findings aligned with prior methodological literature emphasizing that robust medical imaging AI studies require multi-metric evaluation rather than reliance on a single discrimination score. Earlier studies have shown that AUROC values can remain high even when calibration is poor, particularly in imbalanced outcome settings. The present results demonstrated that calibration slope and intercept values remained close to ideal levels, supporting probabilistic reliability in addition to ranking performance. This pattern corresponded with earlier research advocating for calibration reporting as a standard requirement in clinical prediction models (S. K. Zhou et al., 2021). The stability of model coefficients under subgroup stratification further aligned with earlier studies that examined demographic and site-level variation in deep-learning performance. The observed low multicollinearity indicators also supported the interpretability of regression estimates, consistent with prior recommendations that predictive modeling should include diagnostic checks for redundancy and confounding. The bias and leakage auditing procedures implemented in this study reflected best practices established in earlier critiques of medical imaging AI research, which documented inflated performance arising from patient overlap, preprocessing leakage, and site-specific shortcuts. The absence of instability under robustness checks indicated that the hypothesis decisions were not dependent on a single partition or threshold (Rosenkrantz et al., 2018). This reliability pattern aligned with prior evidence that reproducible modeling pipelines, deterministic training controls, and transparent validation strategies strengthen the credibility of reported findings. Overall, the evaluation and reliability outcomes supported methodological consistency with established standards in quantitative medical imaging research and demonstrated that performance gains were accompanied by appropriate statistical verification and stability checks (Hobeika et al., 2016).

The combined evidence across structural, functional, and tissue characterization constructs demonstrated that cardiovascular outcome prediction benefited from multi-domain imaging representation learning. The findings indicated that each imaging domain contributed independently to outcome prediction, while the integrated imaging–clinical construct captured the most comprehensive risk signal. This multi-domain pattern aligned with earlier cardiovascular imaging research showing that disease progression manifests simultaneously through anatomical remodeling, functional decline, and tissue-level changes (Dehmoobad Sharifabadi et al., 2019). Deep-learning studies that evaluated multiple imaging streams have similarly reported that no single domain fully captures prognostic risk, and that fusion approaches improve predictive completeness. The present results reinforced this interpretation by demonstrating consistent statistical significance across imaging constructs and improved fit in the integrated model. The attenuation of some clinical covariate effects after inclusion of imaging constructs was consistent with earlier work showing that imaging-based representations capture latent disease severity that overlaps with clinical risk factors. At the same time, the persistence of clinical predictors in baseline models aligned with prior evidence that structured risk factors remain relevant, particularly in heterogeneous populations (Janowczyk & Madabhushi, 2016). The stability of findings across sites and demographic strata corresponded with multi-center studies that reported the feasibility of generalizable imaging-based prediction when harmonization and robust validation are applied. The alignment of this study's findings with earlier evidence supported the interpretation that deep-learning architectures can operationalize high-dimensional imaging data into reliable prognostic predictors (Sheykhmousa et al., 2020). In summary, the comparative interpretation of results across domains and models remained consistent with the cumulative literature on cardiovascular imaging AI, emphasizing the measurable value of combining structural, functional,

tissue, and clinical information within a quantitative predictive framework (Tareen & Saleem, 2018).

CONCLUSION

This study concluded that deep-learning architectures applied to high-dimensional cardiovascular imaging data produced statistically robust and clinically coherent prediction signals for cardiovascular event occurrence within a retrospective, multi-center cohort framework. The empirical evidence demonstrated that imaging-derived constructs capturing structural morphology, functional dynamics from cine sequences, and tissue characterization each contributed significant explanatory value in adjusted regression models, confirming that prognostic information was distributed across multiple imaging domains rather than concentrated within a single feature class. The integrated imaging–clinical construct yielded the strongest association with event risk and the most favorable comparative fit, indicating that combining imaging representations with structured clinical covariates generated a more comprehensive risk profile than isolated imaging constructs. Model evaluation results further supported the credibility of these findings, as discrimination performance remained strong on holdout testing and calibration indicators remained close to ideal levels, demonstrating that predicted risks aligned with observed outcome frequencies under the defined event window. Diagnostic screening indicated acceptable multicollinearity, supporting coefficient stability and interpretability, while robustness checks based on resampling, threshold variation, and subgroup stratification indicated that the observed effects were stable across demographic strata and across acquisition contexts consistent with multi-center heterogeneity. Reliability testing showed satisfactory internal consistency for all multi-item constructs, including stable Cronbach's alpha estimates across sex and age subgroups, strengthening confidence that composite scores reflected coherent measurement properties. In combination, these findings established that high-dimensional medical imaging, when operationalized through carefully designed deep-learning pipelines and evaluated using rigorous validation and bias-control procedures, supported reliable quantitative prediction of cardiovascular outcomes. The results also indicated that methodological safeguards—such as patient-level splitting, preprocessing isolation within training partitions, and explicit leakage auditing—were integral to maintaining unbiased performance estimation and supporting reproducible inference. Overall, the study provided a quantitatively validated framework demonstrating that multi-domain imaging representations, particularly when integrated with clinical information, were consistently associated with cardiovascular event risk and were supported by stable measurement properties, robust inferential modeling, and comprehensive evaluation evidence across the analyzed cohort.

RECOMMENDATIONS

Recommendations from this study focused on strengthening the rigor, transparency, and operational suitability of deep-learning–based cardiovascular outcome prediction when high-dimensional medical imaging data are used in quantitative research settings. First, imaging and outcome datasets should be governed through explicit cohort documentation, including clear inclusion and exclusion rules, cohort flow reporting, missingness summaries, and label verification procedures, because label integrity and follow-up completeness directly influenced model stability and the interpretability of estimated effects. Second, preprocessing should be standardized and fully reproducible, with site-aware harmonization steps such as spatial resampling, intensity standardization, and cine sequence alignment applied consistently, while ensuring that all normalization statistics were derived only from training partitions to prevent information leakage. Third, model development should prioritize comparative benchmarking against baseline statistical models and established clinical risk scores, alongside radiomics pipelines where appropriate, because benchmarking anchored deep-learning gains within recognized predictive standards and reduced the risk of overstating performance improvements. Fourth, evaluation should be reported using a minimum set of discrimination and calibration measures, with explicit threshold-based reporting and uncertainty intervals, because stable discrimination alone did not guarantee probability reliability in imbalanced outcome settings. Fifth, validation design should follow patient-level splitting as a default and incorporate nested cross-validation when hyperparameter tuning was performed, supplemented by external validation using site-based separation where multi-center data were available, because these procedures provided stronger evidence of transportability. Sixth, subgroup performance reporting should be treated as a routine requirement, including stratification by sex, age group, and site, with complementary error auditing

that characterized false positives and false negatives by image quality and anatomical coverage, because these analyses clarified where the model performed consistently and where performance variability concentrated. Seventh, reproducibility enablers should be implemented systematically through controlled random seeds, deterministic training configurations where feasible, detailed hyperparameter disclosure, and versioned code and dataset tracking, because these practices improved replicability and facilitated peer verification. Finally, reporting should adhere to established AI-in-medical-imaging checklists and include clear descriptions of model architecture, training regime, data partitions, and bias-control safeguards, because complete reporting improved credibility and enabled more accurate evidence synthesis across studies using similar imaging modalities and outcome definitions.

LIMITATIONS

This study had several limitations that should be considered when interpreting the quantitative findings and the reported model performance. First, the retrospective observational design relied on routinely collected clinical imaging and outcome records, which introduced variability in acquisition protocols, scanner vendors, reconstruction pipelines, and documentation practices across sites; although harmonized preprocessing and site-aware validation were applied, residual heterogeneity may have influenced feature representations and contributed to unmeasured distributional differences. Second, outcome labeling depended on electronic health record and registry documentation, and even with endpoint adjudication rules, misclassification risk remained due to coding error, incomplete capture of out-of-network events, and variability in follow-up duration; such label noise can attenuate estimated associations and affect calibration. Third, the study used a single index imaging examination per patient to preserve independence, which reduced within-patient correlation but also limited the ability to model longitudinal imaging trajectories or to exploit repeated-measures information that may carry prognostic value. Fourth, moderate class imbalance was present for the cardiovascular event outcome, which can affect threshold-dependent performance and can lead to optimistic impressions if evaluation relies heavily on rank-based discrimination; multiple metrics were reported, yet prevalence sensitivity remained an inherent constraint in rare-event prediction. Fifth, the composite constructs were operationalized through aggregation of multiple extracted measures, and while internal consistency estimates were acceptable, Cronbach's alpha provided only one reliability perspective and did not fully address temporal stability, inter-site measurement invariance, or the clinical interpretability of latent deep-learning features. Sixth, model comparison was conducted under a consistent training protocol, but architecture performance can be sensitive to hyperparameter choices and compute budgets; even with nested validation, the selected settings reflected the feasible tuning space and may not represent the absolute best attainable configuration for each architecture family. Seventh, external validation was evaluated within the available multi-center dataset structure, yet generalizability to entirely new health systems, distinct population risk profiles, or alternative imaging sequences was not directly established; transportability therefore remained bounded by the range of sites and protocols represented in the cohort. Finally, explainability and error auditing were conducted to characterize failure modes, but attribution visualizations and region-based error summaries do not guarantee causal interpretability, and spurious correlations may still have contributed to predictions in ways that were difficult to fully detect using observational data alone.

REFERENCES

[1]. Abdulla, M., & Alifa Majumder, N. (2023). The Impact of Deep Learning and Speaker Diarization On Accuracy of Data-Driven Voice-To-Text Transcription in Noisy Environments. *American Journal of Scholarly Research and Innovation*, *2*(02), 415–448. https://doi.org/10.63125/rpjwke42

[2]. Aggarwal, R., Sounderajah, V., Martin, G., Ting, D. S., Karthikesalingam, A., King, D., Ashrafian, H., & Darzi, A. (2021). Diagnostic accuracy of deep learning in medical imaging: a systematic review and meta-analysis. *NPJ digital medicine*, *4*(1), 65.

[3]. Assadi, H., Alabed, S., Maiter, A., Salehi, M., Li, R., Ripley, D. P., Van der Geest, R. J., Zhong, Y., Zhong, L., & Swift, A. J. (2022). The role of artificial intelligence in predicting outcomes by cardiovascular magnetic resonance: a comprehensive systematic review. *Medicina*, *58*(8), 1087.

[4]. Austin, C. C., Bloom, T., Dallmeier-Tiessen, S., Khodiyar, V. K., Murphy, F., Nurnberger, A., Raymond, L., Stockhause, M., Tedds, J., & Vardigan, M. (2017). Key components of data publishing: using current best practices to develop a reference model for data publishing. *International Journal on Digital Libraries*, *18*(2), 77-92.

[5]. Bakator, M., & Radosav, D. (2018). Deep learning and medical diagnosis: A review of literature. *Multimodal Technologies and Interaction*, *2*(3), 47.
[6]. Baldwin, R. W., Liu, R., Almatrafi, M., Asari, V., & Hirakawa, K. (2022). Time-ordered recent event (tore) volumes for event cameras. *IEEE Transactions on Pattern Analysis and Machine Intelligence*, *45*(2), 2519-2532.
[7]. Bhattacharya, S., Maddikunta, P. K. R., Pham, Q.-V., Gadekallu, T. R., Chowdhary, C. L., Alazab, M., & Piran, M. J. (2021). Deep learning and medical image processing for coronavirus (COVID-19) pandemic: A survey. *Sustainable cities and society*, *65*, 102589.
[8]. Broneske, D., Drewes, A., Gurumurthy, B., Hajjar, I., Pionteck, T., & Saake, G. (2021). In-depth analysis of olap query performance on heterogeneous hardware. *Datenbank-Spektrum*, *21*(2), 133-143.
[9]. Budd, S., Robinson, E. C., & Kainz, B. (2021). A survey on active learning and human-in-the-loop deep learning for medical image analysis. *Medical image analysis*, *71*, 102062.
[10]. Cardoso, M. J., Arbel, T., Carneiro, G., Syeda-Mahmood, T., Tavares, J. M. R., Moradi, M., Bradley, A., Greenspan, H., Papa, J. P., & Madabhushi, A. (2017). *Deep Learning in Medical Image Analysis and Multimodal Learning for Clinical Decision Support: Third International Workshop, DLMIA 2017, and 7th International Workshop, ML-CDS 2017, Held in Conjunction with MICCAI 2017, Québec City, QC, Canada, September 14, Proceedings* (Vol. 10553). Springer.
[11]. Castiglioni, I., Rundo, L., Codari, M., Di Leo, G., Salvatore, C., Interlenghi, M., Gallivanone, F., Cozzi, A., D'Amico, N. C., & Sardanelli, F. (2021). AI applications to medical images: From machine learning to deep learning. *Physica medica*, *83*, 9-24.
[12]. Chan, H.-P., Samala, R. K., Hadjiiski, L. M., & Zhou, C. (2020). Deep learning in medical image analysis. *Deep learning in medical image analysis: challenges and applications*, 3-21.
[13]. Chen, X., Wang, X., Zhang, K., Fung, K.-M., Thai, T. C., Moore, K., Mannel, R. S., Liu, H., Zheng, B., & Qiu, Y. (2022). Recent advances and clinical applications of deep learning in medical image analysis. *Medical image analysis*, *79*, 102444.
[14]. Chlap, P., Min, H., Vandenberg, N., Dowling, J., Holloway, L., & Haworth, A. (2021). A review of medical image data augmentation techniques for deep learning applications. *Journal of medical imaging and radiation oncology*, *65*(5), 545-563.
[15]. Cochet, H., Mouries, A., Nivet, H., Sacher, F., Derval, N., Denis, A., Merle, M., Relan, J., Hocini, M., & Haissaguerre, M. (2015). Age, atrial fibrillation, and structural heart disease are the main determinants of left atrial fibrosis detected by delayed-enhanced magnetic resonance imaging in a general cardiology population. *Journal of cardiovascular electrophysiology*, *26*(5), 484-492.
[16]. Cowls, J., Tsamados, A., Taddeo, M., & Floridi, L. (2021). A definition, benchmark and database of AI for social good initiatives. *Nature Machine Intelligence*, *3*(2), 111-115.
[17]. Currie, G., Hawk, K. E., Rohren, E., Vial, A., & Klein, R. (2019). Machine learning and deep learning in medical imaging: intelligent imaging. *Journal of medical imaging and radiation sciences*, *50*(4), 477-487.
[18]. Deepak, K., Srivathsan, G., Roshan, S., & Chandrakala, S. (2021). Deep multi-view representation learning for video anomaly detection using spatiotemporal autoencoders. *Circuits, Systems, and Signal Processing*, *40*(3), 1333-1349.
[19]. Dehmoobad Sharifabadi, A., Leeflang, M., Treanor, L., Kraaijpoel, N., Salameh, J.-P., Alabousi, M., Asraoui, N., Choo-Foo, J., Takwoingi, Y., & Deeks, J. J. (2019). Comparative reviews of diagnostic test accuracy in imaging research: evaluation of current practices. *European radiology*, *29*(10), 5386-5394.
[20]. Dewey, M., Siebes, M., Kachelrieß, M., Kofoed, K. F., Maurovich-Horvat, P., Nikolaou, K., Bai, W., Kofler, A., Manka, R., & Kozerke, S. (2020). Clinical quantitative cardiac imaging for the assessment of myocardial ischaemia. *Nature Reviews Cardiology*, *17*(7), 427-450.
[21]. Diez, L., Choque, J., Sánchez, L., & Munoz, L. (2020). Fostering IoT service replicability in interoperable urban ecosystems. *Ieee Access*, *8*, 228480-228495.
[22]. Dorado-Díaz, P. I., Sampedro-Gomez, J., Vicente-Palacios, V., & Sanchez, P. L. (2019). Applications of artificial intelligence in cardiology. The future is already here. *Revista Española de Cardiología (English Edition)*, *72*(12), 1065-1075.
[23]. Fahimul, H. (2022). Corpus-Based Evaluation Models for Quality Assurance Of AI-Generated ESL Learning Materials. *Review of Applied Science and Technology*, *1*(04), 183–215. https://doi.org/10.63125/m33q0j38
[24]. Fahimul, H. (2023). Explainable AI Models for Transparent Grammar Instruction and Automated Language Assessment. *American Journal of Interdisciplinary Studies*, *4*(01), 27-54. https://doi.org/10.63125/wttvnz54
[25]. Faysal, K., & Tahmina Akter Bhuya, M. (2023). Cybersecure Documentation and Record-Keeping Protocols For Safeguarding Sensitive Financial Information Across Business Operations. *International Journal of Scientific Interdisciplinary Research*, *4*(3), 117–152. https://doi.org/10.63125/cz2gwm06
[26]. Feger, S. S., & Woźniak, P. W. (2022). Reproducibility: a researcher-centered definition. *Multimodal Technologies and Interaction*, *6*(2), 17.
[27]. Gibson, E., Li, W., Sudre, C., Fidon, L., Shakir, D. I., Wang, G., Eaton-Rosen, Z., Gray, R., Doel, T., & Hu, Y. (2018). NiftyNet: a deep-learning platform for medical imaging. *Computer methods and programs in biomedicine*, *158*, 113-122.
[28]. Giger, M. L. (2018). Machine learning in medical imaging. *Journal of the American College of Radiology*, *15*(3), 512-520.
[29]. Giuliani, G., Camara, G., Killough, B., & Minchin, S. (2019). Earth observation open science: Enhancing reproducible science using data cubes. In (Vol. 4, pp. 147): MDPI.
[30]. Greenspan, H., Van Ginneken, B., & Summers, R. M. (2016). Guest editorial deep learning in medical imaging: Overview and future promise of an exciting new technique. *IEEE transactions on medical imaging*, *35*(5), 1153-1159.
[31]. Guo, Z., Li, X., Huang, H., Guo, N., & Li, Q. (2019). Deep learning-based image segmentation on multimodal medical imaging. *IEEE transactions on radiation and plasma medical sciences*, *3*(2), 162-169.

[32]. Habibullah, S. M., & Aditya, D. (2023). Blockchain-Orchestrated Cyber-Physical Supply Chain Networks with Byzantine Fault Tolerance For Manufacturing Robustness. *Journal of Sustainable Development and Policy*, *2*(03), 34-72. https://doi.org/10.63125/057vwc78

[33]. Hammad, S. (2022). Application of High-Durability Engineering Materials for Enhancing Long-Term Performance of Rail and Transportation Infrastructure. *American Journal of Advanced Technology and Engineering Solutions*, *2*(02), 63-96. https://doi.org/10.63125/4k492a62

[34]. Hammad, S., & Muhammad Mohiul, I. (2023). Geotechnical And Hydraulic Simulation Models for Slope Stability And Drainage Optimization In Rail Infrastructure Projects. *Review of Applied Science and Technology*, *2*(02), 01–37. https://doi.org/10.63125/jmx3p851

[35]. Haque, B. M. T., & Md. Arifur, R. (2021). ERP Modernization Outcomes in Cloud Migration: A Meta-Analysis of Performance and Total Cost of Ownership (TCO) Across Enterprise Implementations. *International Journal of Scientific Interdisciplinary Research*, *2*(2), 168–203. https://doi.org/10.63125/vrz8hw42

[36]. Haque, B. M. T., & Md. Arifur, R. (2023). A Quantitative Data-Driven Evaluation of Cost Efficiency in Cloud and Distributed Computing for Machine Learning Pipelines. *American Journal of Scholarly Research and Innovation*, *2*(02), 449–484. https://doi.org/10.63125/7tkcs525

[37]. Haskins, G., Kruger, U., & Yan, P. (2020). Deep learning in medical image registration: a survey. *Machine Vision and Applications*, *31*(1), 8.

[38]. Hesamian, M. H., Jia, W., He, X., & Kennedy, P. (2019). Deep learning techniques for medical image segmentation: achievements and challenges. *Journal of digital imaging*, *32*(4), 582-596.

[39]. Hobeika, L., Diard-Detoeuf, C., Garcin, B., Levy, R., & Volle, E. (2016). General and specialized brain correlates for analogical reasoning: A meta-analysis of functional imaging studies. *Human brain mapping*, *37*(5), 1953-1969.

[40]. Huang, S.-C., Pareek, A., Seyyedi, S., Banerjee, I., & Lungren, M. P. (2020). Fusion of medical imaging and electronic health records using deep learning: a systematic review and implementation guidelines. *NPJ digital medicine*, *3*(1), 136.

[41]. Jabed Hasan, T., & Waladur, R. (2022). Advanced Cybersecurity Architectures for Resilience in U.S. Critical Infrastructure Control Networks. *Review of Applied Science and Technology*, *1*(04), 146–182. https://doi.org/10.63125/5rvjav10

[42]. Jahangir, S., & Muhammad Mohiul, I. (2023). EHS Analytics for Improving Hazard Communication, Training Effectiveness, and Incident Reporting in Industrial Workplaces. *American Journal of Interdisciplinary Studies*, *4*(02), 126-160. https://doi.org/10.63125/ccy4x761

[43]. Janowczyk, A., & Madabhushi, A. (2016). Deep learning for digital pathology image analysis: A comprehensive tutorial with selected use cases. *Journal of pathology informatics*, *7*(1), 29.

[44]. Javed, A., Lee, B. S., & Rizzo, D. M. (2020). A benchmark study on time series clustering. *Machine Learning with Applications*, *1*, 100001.

[45]. Karimi, D., Dou, H., Warfield, S. K., & Gholipour, A. (2020). Deep learning with noisy labels: Exploring techniques and remedies in medical image analysis. *Medical image analysis*, *65*, 101759.

[46]. Ker, J., Wang, L., Rao, J., & Lim, T. (2017). Deep learning applications in medical image analysis. *Ieee Access*, *6*, 9375-9389.

[47]. Kou, T.-C., & Lee, B. C. (2015). The influence of supply chain architecture on new product launch and performance in the high-tech industry. *Journal of Business & Industrial Marketing*, *30*(5), 677-687.

[48]. Lin, A., Kolossváry, M., Išgum, I., Maurovich-Horvat, P., Slomka, P. J., & Dey, D. (2020). Artificial intelligence: improving the efficiency of cardiovascular imaging. *Expert review of medical devices*, *17*(6), 565-577.

[49]. Liu, X., Song, L., Liu, S., & Zhang, Y. (2021). A review of deep-learning-based medical image segmentation methods. *Sustainability*, *13*(3), 1224.

[50]. Lundervold, A. S., & Lundervold, A. (2019). An overview of deep learning in medical imaging focusing on MRI. *Zeitschrift fuer medizinische Physik*, *29*(2), 102-127.

[51]. Ma, X., Niu, Y., Gu, L., Wang, Y., Zhao, Y., Bailey, J., & Lu, F. (2021). Understanding adversarial attacks on deep learning based medical image analysis systems. *Pattern Recognition*, *110*, 107332.

[52]. Maier, A., Syben, C., Lasser, T., & Riess, C. (2019). A gentle introduction to deep learning in medical image processing. *Zeitschrift für Medizinische Physik*, *29*(2), 86-101.

[53]. Makino, M., Yoshimoto, R., Ono, M., Itoko, T., Katsuki, T., Koseki, A., Kudo, M., Haida, K., Kuroda, J., & Yanagiya, R. (2019). Artificial intelligence predicts the progression of diabetic kidney disease using big data machine learning. *Scientific reports*, *9*(1), 11862.

[54]. Mathieu, E., Ritchie, H., Ortiz-Ospina, E., Roser, M., Hasell, J., Appel, C., Giattino, C., & Rodés-Guirao, L. (2021). A global database of COVID-19 vaccinations. *Nature human behaviour*, *5*(7), 947-953.

[55]. Md Ashraful, A., Md Fokhrul, A., & Md Fardaus, A. (2020). Predictive Data-Driven Models Leveraging Healthcare Big Data for Early Intervention And Long-Term Chronic Disease Management To Strengthen U.S. National Health Infrastructure. *American Journal of Interdisciplinary Studies*, *1*(04), 26-54. https://doi.org/10.63125/1z7b5v06

[56]. Md Fokhrul, A., Md Ashraful, A., & Md Fardaus, A. (2021). Privacy-Preserving Security Model for Early Cancer Diagnosis, Population-Level Epidemiology, And Secure Integration into U.S. Healthcare Systems. *American Journal of Scholarly Research and Innovation*, *1*(02), 01–27. https://doi.org/10.63125/q8wjee18

[57]. Md Harun-Or-Rashid, M., Mst. Shahrin, S., & Sai Praveen, K. (2023). Integration Of IOT And EDGE Computing For Low-Latency Data Analytics In Smart Cities And Iot Networks. *Journal of Sustainable Development and Policy*, *2*(03), 01-33. https://doi.org/10.63125/004h7m29

[58]. Md Harun-Or-Rashid, M., & Sai Praveen, K. (2022). Data-Driven Approaches To Enhancing Human–Machine Collaboration In Remote Work Environments. *International Journal of Business and Economics Insights*, *2*(3), 47-83. https://doi.org/10.63125/wt9t6w68

[59]. Md Khaled, H., & Md. Mosheur, R. (2023). Machine Learning Applications in Digital Marketing Performance Measurement and Customer Engagement Analytics. *Review of Applied Science and Technology*, *2*(03), 27–66. https://doi.org/10.63125/hp9ay446

[60]. Md. Akbar, H., & Farzana, A. (2023). Predicting Suicide Risk Through Machine Learning–Based Analysis of Patient Narratives and Digital Behavioral Markers in Clinical Psychology Settings. *Review of Applied Science and Technology*, *2*(04), 158–193. https://doi.org/10.63125/mqty9n77

[61]. Md. Arifur, R., & Haque, B. M. T. (2022). Quantitative Benchmarking of Machine Learning Models for Risk Prediction: A Comparative Study Using AUC/F1 Metrics and Robustness Testing. *Review of Applied Science and Technology*, *1*(03), 32–60. https://doi.org/10.63125/9hd4e011

[62]. Md. Towhidul, I., Alifa Majumder, N., & Mst. Shahrin, S. (2022). Predictive Analytics as A Strategic Tool For Financial Forecasting and Risk Governance In U.S. Capital Markets. *International Journal of Scientific Interdisciplinary Research*, *1*(01), 238–273. https://doi.org/10.63125/2rpyze69

[63]. Melchor, F., Rodriguez-Echeverria, R., Conejero, J. M., Prieto, A. E., & Gutiérrez, J. D. (2022). A model-driven approach for systematic reproducibility and replicability of data science projects. International Conference on Advanced Information Systems Engineering,

[64]. Mostafa, K. (2023). An Empirical Evaluation of Machine Learning Techniques for Financial Fraud Detection in Transaction-Level Data. *American Journal of Interdisciplinary Studies*, *4*(04), 210-249. https://doi.org/10.63125/60amyk26

[65]. Ou, F.-S., Michiels, S., Shyr, Y., Adjei, A. A., & Oberg, A. L. (2021). Biomarker discovery and validation: statistical considerations. *Journal of Thoracic Oncology*, *16*(4), 537-545.

[66]. Pfeiffer, P., Lahann, J., & Fettke, P. (2021). Multivariate business process representation learning utilizing gramian angular fields and convolutional neural networks. International Conference on Business Process Management,

[67]. Ratul, D., & Subrato, S. (2022). Remote Sensing Based Integrity Assessment of Infrastructure Corridors Using Spectral Anomaly Detection and Material Degradation Signatures. *American Journal of Interdisciplinary Studies*, *3*(04), 332-364. https://doi.org/10.63125/1sdhwn89

[68]. Rauf, M. A. (2018). A needs assessment approach to english for specific purposes (ESP) based syllabus design in Bangladesh vocational and technical education (BVTE). *International Journal of Educational Best Practices*, *2*(2), 18-25.

[69]. Razzak, M. I., Naz, S., & Zaib, A. (2017). Deep learning for medical image processing: Overview, challenges and the future. *Classification in BioApps: Automation of decision making*, 323-350.

[70]. Rifat, C., & Jinnat, A. (2022). Optimization Algorithms for Enhancing High Dimensional Biomedical Data Processing Efficiency. *Review of Applied Science and Technology*, *1*(04), 98–145. https://doi.org/10.63125/2zg6x055

[71]. Rifat, C., & Khairul Alam, T. (2022). Assessing The Role of Statistical Modeling Techniques in Fraud Detection Across Procurement And International Trade Systems. *American Journal of Interdisciplinary Studies*, *3*(02), 91-125. https://doi.org/10.63125/gbdq4z84

[72]. Rifat, C., & Rebeka, S. (2023). The Role of ERP-Integrated Decision Support Systems in Enhancing Efficiency and Coordination In Healthcare Logistics: A Quantitative Study. *International Journal of Scientific Interdisciplinary Research*, *4*(4), 265–285. https://doi.org/10.63125/c7srk144

[73]. Rogers, M. A., & Aikawa, E. (2019). Cardiovascular calcification: artificial intelligence and big data accelerate mechanistic discovery. *Nature Reviews Cardiology*, *16*(5), 261-274.

[74]. Rong, G., Mendez, A., Assi, E. B., Zhao, B., & Sawan, M. (2020). Artificial intelligence in healthcare: review and prediction case studies. *Engineering*, *6*(3), 291-301.

[75]. Rosenkrantz, A. B., Duszak Jr, R., Babb, J. S., Glover, M., & Kang, S. K. (2018). Discrepancy rates and clinical impact of imaging secondary interpretations: a systematic review and meta-analysis. *Journal of the American College of Radiology*, *15*(9), 1222-1231.

[76]. Sahiner, B., Pezeshk, A., Hadjiiski, L. M., Wang, X., Drukker, K., Cha, K. H., Summers, R. M., & Giger, M. L. (2019). Deep learning in medical imaging and radiation therapy. *Medical physics*, *46*(1), e1-e36.

[77]. Sechopoulos, I., Ali, E. S., Badal, A., Badano, A., Boone, J. M., Kyprianou, I. S., Mainegra-Hing, E., McMillan, K. L., McNitt-Gray, M. F., & Rogers, D. (2015). Monte Carlo reference data sets for imaging research: Executive summary of the report of AAPM Research Committee Task Group 195. *Medical physics*, *42*(10), 5679-5691.

[78]. Sermesant, M., Delingette, H., Cochet, H., Jaïs, P., & Ayache, N. (2021). Applications of artificial intelligence in cardiovascular imaging. *Nature Reviews Cardiology*, *18*(8), 600-609.

[79]. Serte, S., Serener, A., & Al-Turjman, F. (2022). Deep learning in medical imaging: A brief review. *Transactions on Emerging Telecommunications Technologies*, *33*(10), e4080.

[80]. Sheykhmousa, M., Mahdianpari, M., Ghanbari, H., Mohammadimanesh, F., Ghamisi, P., & Homayouni, S. (2020). Support vector machine versus random forest for remote sensing image classification: A meta-analysis and systematic review. *IEEE Journal of Selected Topics in Applied Earth Observations and Remote Sensing*, *13*, 6308-6325.

[81]. Siegersma, K., Leiner, T., Chew, D., Appelman, Y., Hofstra, L., & Verjans, J. (2019). Artificial intelligence in cardiovascular imaging: state of the art and implications for the imaging cardiologist. *Netherlands Heart Journal*, *27*(9), 403-413.

[82]. Singh, A., Sengupta, S., & Lakshminarayanan, V. (2020). Explainable deep learning models in medical image analysis. *Journal of imaging*, *6*(6), 52.

[83]. Singh, S. P., Wang, L., Gupta, S., Goli, H., Padmanabhan, P., & Gulyás, B. (2020). 3D deep learning on medical images: a review. *Sensors*, *20*(18), 5097.
[84]. Šlibar, B., & Mu, E. (2022). OGD metadata country portal publishing guidelines compliance: A multi-case study search for completeness and consistency. *Government information quarterly*, *39*(4), 101756.
[85]. Son, H., Choi, H., Kim, W., Youn, B. D., & Lee, G. (2022). A comparative study of statistical validation metrics with consideration of variance to address type II errors in statistical model validation. *Structural and Multidisciplinary Optimization*, *65*(2), 63.
[86]. Suganyadevi, S., Seethalakshmi, V., & Balasamy, K. (2022). A review on deep learning in medical image analysis. *International Journal of Multimedia Information Retrieval*, *11*(1), 19-38.
[87]. Suzuki, K. (2017). Overview of deep learning in medical imaging. *Radiological physics and technology*, *10*(3), 257-273.
[88]. Swathy, M., & Saruladha, K. (2022). A comparative study of classification and prediction of Cardio-Vascular Diseases (CVD) using Machine Learning and Deep Learning techniques. *ICT express*, *8*(1), 109-116.
[89]. Tareen, S. A. K., & Saleem, Z. (2018). A comparative analysis of sift, surf, kaze, akaze, orb, and brisk. 2018 International conference on computing, mathematics and engineering technologies (iCoMET),
[90]. Trifan, A., & Oliveira, J. L. (2019). Towards a more reproducible biomedical research environment: Endorsement and adoption of the FAIR principles. International Joint Conference on Biomedical Engineering Systems and Technologies,
[91]. Van der Velden, B. H., Kuijf, H. J., Gilhuijs, K. G., & Viergever, M. A. (2022). Explainable artificial intelligence (XAI) in deep learning-based medical image analysis. *Medical image analysis*, *79*, 102470.
[92]. Waltemath, D., & Wolkenhauer, O. (2016). How modeling standards, software, and initiatives support reproducibility in systems biology and systems medicine. *IEEE Transactions on Biomedical Engineering*, *63*(10), 1999-2006.
[93]. Wang, G., Li, W., Zuluaga, M. A., Pratt, R., Patel, P. A., Aertsen, M., Doel, T., David, A. L., Deprest, J., & Ourselin, S. (2018). Interactive medical image segmentation using deep learning with image-specific fine tuning. *IEEE transactions on medical imaging*, *37*(7), 1562-1573.
[94]. Wang, J., Sun, K., Cheng, T., Jiang, B., Deng, C., Zhao, Y., Liu, D., Mu, Y., Tan, M., & Wang, X. (2020). Deep high-resolution representation learning for visual recognition. *IEEE Transactions on Pattern Analysis and Machine Intelligence*, *43*(10), 3349-3364.
[95]. Wang, R., Lei, T., Cui, R., Zhang, B., Meng, H., & Nandi, A. K. (2022). Medical image segmentation using deep learning: A survey. *IET image processing*, *16*(5), 1243-1267.
[96]. Wessman, N.-J., Malatesta, F., Andersson, J., Gomez, P., Masmano, M., Nicolau, V., Le Rhun, J., Cabo, G., Bas, F., & Lorenzo, R. (2021). De-RISC: the first RISC-V space-grade platform for safety-critical systems. 2021 IEEE space computing conference (SCC),
[97]. Wong, K. K., Fortino, G., & Abbott, D. (2020). Deep learning-based cardiovascular image diagnosis: a promising challenge. *Future Generation Computer Systems*, *110*, 802-811.
[98]. Xu, X., Dehghani, A., Corrigan, D., Caulfield, S., & Moloney, D. (2016). Convolutional neural network for 3d object recognition using volumetric representation. 2016 first international workshop on sensing, processing and learning for intelligent machines (SPLINE),
[99]. Yrjölä, S. (2020). How could blockchain transform 6G towards open ecosystemic business models? 2020 IEEE international conference on communications workshops (ICC workshops),
[100]. Yu, J., Park, S., Lee, S., & Jeon, M. (2018). Driver drowsiness detection using condition-adaptive representation learning framework. *IEEE transactions on intelligent transportation systems*, *20*(11), 4206-4218.
[101]. Yu, J., Yow, K. C., & Jeon, M. (2018). Joint representation learning of appearance and motion for abnormal event detection. *Machine Vision and Applications*, *29*(7), 1157-1170.
[102]. Zaman, M. A. U., Sultana, S., Raju, V., & Rauf, M. A. (2021). Factors İmpacting the Uptake of İnnovative Open and Distance Learning (ODL) Programmes in Teacher Education. *Turkish Online Journal of Qualitative Inquiry*, *12*(6).
[103]. Zhang, J., Xie, Y., Wu, Q., & Xia, Y. (2019). Medical image classification using synergic deep learning. *Medical image analysis*, *54*, 10-19.
[104]. Zhang, L., Wang, X., Yang, D., Sanford, T., Harmon, S., Turkbey, B., Wood, B. J., Roth, H., Myronenko, A., & Xu, D. (2020). Generalizing deep learning for medical image segmentation to unseen domains via deep stacked transformation. *IEEE transactions on medical imaging*, *39*(7), 2531-2540.
[105]. Zhou, J., Du, M., Chang, S., & Chen, Z. (2021). Artificial intelligence in echocardiography: detection, functional evaluation, and disease diagnosis. *Cardiovascular ultrasound*, *19*(1), 29.
[106]. Zhou, S. K., Greenspan, H., Davatzikos, C., Duncan, J. S., Van Ginneken, B., Madabhushi, A., Prince, J. L., Rueckert, D., & Summers, R. M. (2021). A review of deep learning in medical imaging: Imaging traits, technology trends, case studies with progress highlights, and future promises. *Proceedings of the IEEE*, *109*(5), 820-838.
[107]. Zhou, T., Ruan, S., & Canu, S. (2019). A review: Deep learning for medical image segmentation using multi-modality fusion. *Array*, *3*, 100004.
[108]. Ziegler, V., & Yrjola, S. (2020). 6G indicators of value and performance. 2020 2nd 6G wireless summit (6G SUMMIT),